760
3C 31-79

HQ. 2365

COO-2908-4

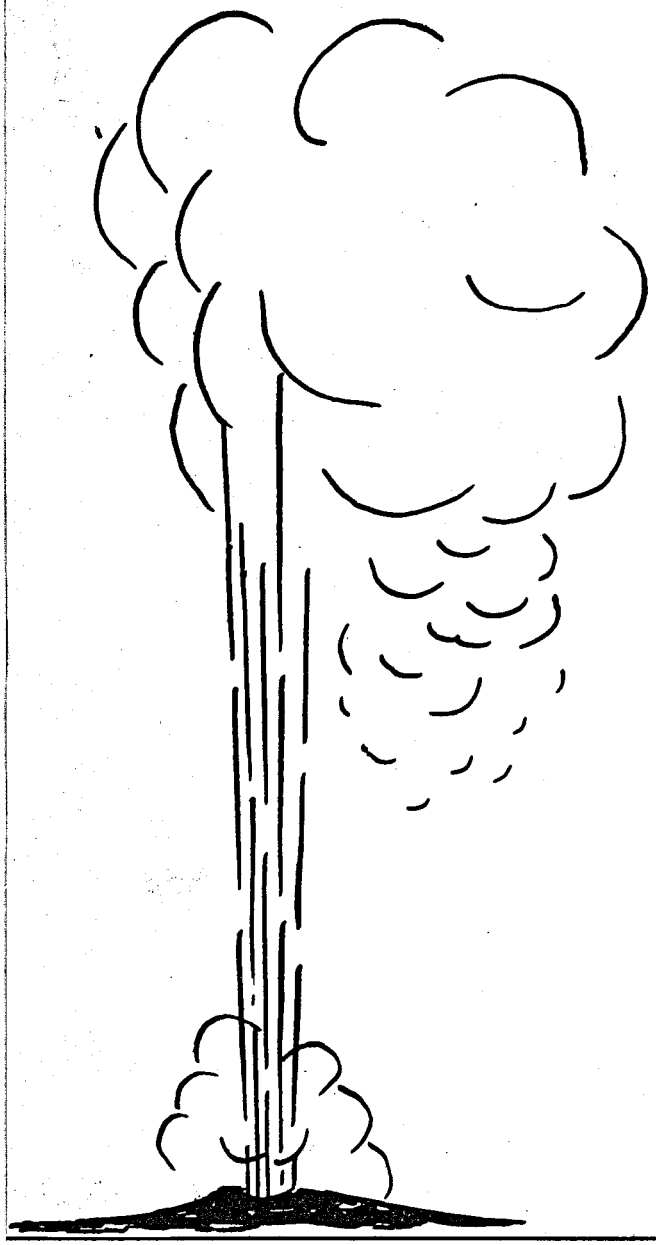

RESEARCH ON THE PHYSICAL PROPERTIES OF GEOTHERMAL RESERVOIR ROCK

Quarterly Report

By
C. K. Skokan
A. Ibrahim

July 1978

Work Performed Under Contract No. EY-76-S-02-2908

Department of Geophysics
Colorado School of Mines
Golden, Colorado

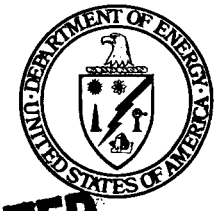

U. S. DEPARTMENT OF ENERGY

Geothermal Energy

DISCLAIMER

NOTICE

COO-2908-4
Distribution Category UC-66a

Colorado School of Mines
Department of Geophysics
Golden, Colorado 80401

Quarterly Report - July, 1978

Research on the Physical Properties of Geothermal Reservoir Rock

U.S. Department of Energy
Contract EY-76-S-02-2908

Investigators: G.V. Keller, L.T. Grose, G.R. Pickett

Report prepared by:
C.K. Skokan and A. Ibrahim

TABLE OF CONTENTS

LIST OF FIGURES

ABSTRACT

Laboratory measurements of thermal conductivity and capillary pressure have been undertaken for samples of Cenozoic Volcanic rocks collected from the Columbia Plateau Volcanic basin. These measurements were performed at atmospheric pressure and room temperature.

Various methods of measuring thermal conductivity were investigated and finally a flash method was chosen. The equipment was constructed and tested. The results were favorable.

Numerous capillary pressure curves were obtained by use of the mercury injection technique. These curves indicate pore structure: pore size, pore distribution, pore volume, and pore geometry. Measurements of this type help to explain variations in rock properties such as seismic velocities and resistivities.

INTRODUCTION

Research on the physical properties of geothermal reservoir rocks at the Colorado School of Mines has progressed in two specific areas:

1). Construction and testing of a flash tube instrument to measure thermal conductivity at room temperature and atmospheric pressure.

2) Preparation of numerous samples and measurement of capillary pressure using the mercury injection technique. These measurements were made at room temperature, as well. The purpose of the capillary pressure measurements is to indicate pore structure. Pore structure directly influences seismic velocities and resistivities in samples. It was hoped that these measurements would explain variations in these properties that were found in previous sections of this research project.

THERMAL CONDUCTIVITY MEASUREMENTS

The measurement of thermal conductivity of the host rock is most important in a geothermal reservoir. First, thermal conductivity gives a good estimate of heat flow in the geothermal system. Secondly, and particularly in hot dry systems, this measurement indicates the amount of heat exchange expected from rock to fluid.

BACKGROUND

The thermal conductivity of porous materials has been extensively treated in literature, theoretically, as well as experimentally. Such studies indicated that thermal conductivity of porous rocks depend on porosity, pore configuration and size, chemical composition of rock matrix, temperature, pressure, saturating fluid conductivity.

Several mathematical models have been introduced to relate the effective thermal conductivity of a porous rock to the above listed parameters. The series, parallel, and geometric mean, are without theoretical foundation. Maxwell's equation (1904) which relates electrical conductivity of a random distribution of solid spheres has been modified by de Vries (1952) to produce an equation for the calculation of thermal conductivity of unconsolidated soil. Kuni, 1960; Wyllie, 1954, and Russell, 1934, developed thermal conductivity equations which relate porosity, conductivities of solid and liquid phases to effective conductivity. Woodside (I & II), 1961, calculated effective thermal conductivity of rock aggregates and cemented rocks and concluded that the geometric mean equation predicts sandstone conductivities which are in good agreement with measured values. Beck, 1976, extended the

range of Maxwell's equation to cover higher porosity and higher conductivity ratios

$$\left(\frac{R_{solid}}{R_{fluid}}\right).$$

Experimental investigations on the effect of porosity, pressure, saturation, and nature of saturant on thermal conductivity of rocks has been carried out on numerous rock varieties. Woodside II, 1961; Sugawara, 1962; Zierfuss, 1956; and Hutt, 1968, indicated a decrease in conductivity of sandstones with increase in porosity for both saturated and dry samples.

Sugawara indicates that thermal conductivity of dry sandstone and brick increases by water saturation. Woodside II, 1961, also found that thermal conductivity of liquid saturated sandstone (water or n-heptane) is greater than that of gas saturated rock (He or N_2O). Zierfuss, 1956, indicated an increase in thermal conductivity of sandstone and limestone samples with increase in water saturation.

Pressure affects thermal conductivities of porous rocks. Generally, the intrinsic thermal conductivity of most rocks (matrix conductivity) is of the same order of magnitude or higher than that of common saturating fluids. Fluid content increases thermal conductivity. In liquid saturated igneous rocks where crack porosity is common, an increase in pressure decreases crack porosity, and decreases thermal conductivity. In dry igneous rocks, pressure closes cracks which represent barriers to heat flow and a subsequent increase in conductivity results (Woodside, 1961). At high pressures, when all forms of porosity is destroyed, effective thermal conductivity approaches the intrinsic conductivity of the rock matrix (Walsh, 1966, Clark, 1941). In partially saturated rocks, an increase in pressure have the expected results of increasing conductivity. Woodside II, 1961, reported an increase in conductivity of sandstone with an increase in confining air pressure.

METHODS OF MEASUREMENT

Classically two methods for measurement of thermal conductivity have been employed: 1) a steady-state method, and 2) a transient or probe method. Because of the drawbacks of both of these methods in measuring thermal conductivity of saturated hard rock samples, a third method, a flash method, has been tested and shows great promise.

When measuring thermal conductivity with the steady state method, either a constant temperature drop (Suss, 1971) or a constant heat flux (Birch method, 1940) is maintained across a standard material, for which the thermal properties are well known, and the unknown sample. Measurements of the steady state heat flux and temperature gradient are made across these two materials which are in series. The shape of the sample must be simple so that the differential equation describing heat conduction may be easily solved.

There are numerous problems encountered when making thermal conductivity measurements with steady state techniques. First, it is difficult to find good insulating material. Therefore edge effects can introduce inaccuracies. Second, a long period of time is required to let the sample come to equilibrium so that a measurement can be made. Third is the problem of surface heat losses over a long period of time. Finally there is a problem in contact resistance.

The transient or probe method overcomes one of the problems encountered with the steady-state technique: this method is much faster. The technique calls for a wire, heated with a constant electrical current, and a thermocouple, thermistor, or resistance thermometer. These items are placed next to each other on a sample or are combined in a "probe". Measurements of

change in temperature with time are made and thermal conductivity is then calculated from the transient curve. Although excellent for some materials, probe measurements on water saturated hard rocks are difficult. The largest problem is that of contact resistance between the probe and sample. As before there are also surface heat losses. Thirdly, the theory accompanying the probe technique applies to infinite sample geometry so it may be necessary to make measurements on very large samples. Finally, the actual probe geometry may introduce errors (Woodside, p. 1692) although many may be compensated for (Blackwell, 1956).

FLASH METHOD

In search of a better technique to measure thermal conductivity of water saturated rocks, the flash technique was investigated. This method previously tested mostly on metals shows great promise in the measurement of thermal conductivity of rocks. The method is very quick; if samples are disk shaped heat loss is minimized, and the problem of contact resistance is eliminated.

A flash method was tested to measure the thermal diffusivity of water saturated samples. A model 503, General Electric Flash Tube, which is capable of generating up to 1000 joules per pulse, was used for this purpose.

Carslaw and Jaeger (1959) developed the theory for heat distribution in a circular plate of material of thickness L when irradiated with a thermal pulse of short duration incident on one of the faces. Their equation is as follows:

$$T(x,t) = \frac{1}{L}\int_0^L T(x,o)dx + \frac{2}{L}\sum_{n=1}^{\infty} \exp\left(\frac{-n^2\pi\alpha t}{L}\right) \cos\frac{n\pi x}{L} \int_0^L T(x_1 o) \cos\frac{n\pi x}{L}\, dx$$

where α is thermal diffusivity in cm^2/sec, T is temperature in ^oC, t is time in seconds, and x is distance in sample parallel to flow of heat. If a pulse of radiant energy is instantaneously and uniformly absorbed in a small depth of sample's front end, then applying the initial conditions and integrating yields:

$$V = 1 + 2 \sum_{n=1}^{\infty} (-1)^n \exp(-n^2 w) \qquad (1)$$

where

$$V = \frac{T(L,t)}{T_M} \quad \text{and} \quad W = \pi^2 \alpha t / L^2$$

$T(L,t)$ is temperature at back surface of sample at time t

T_M is maximum temperature reached at back surface

A plot of equation 1 is shown in Figure 1:

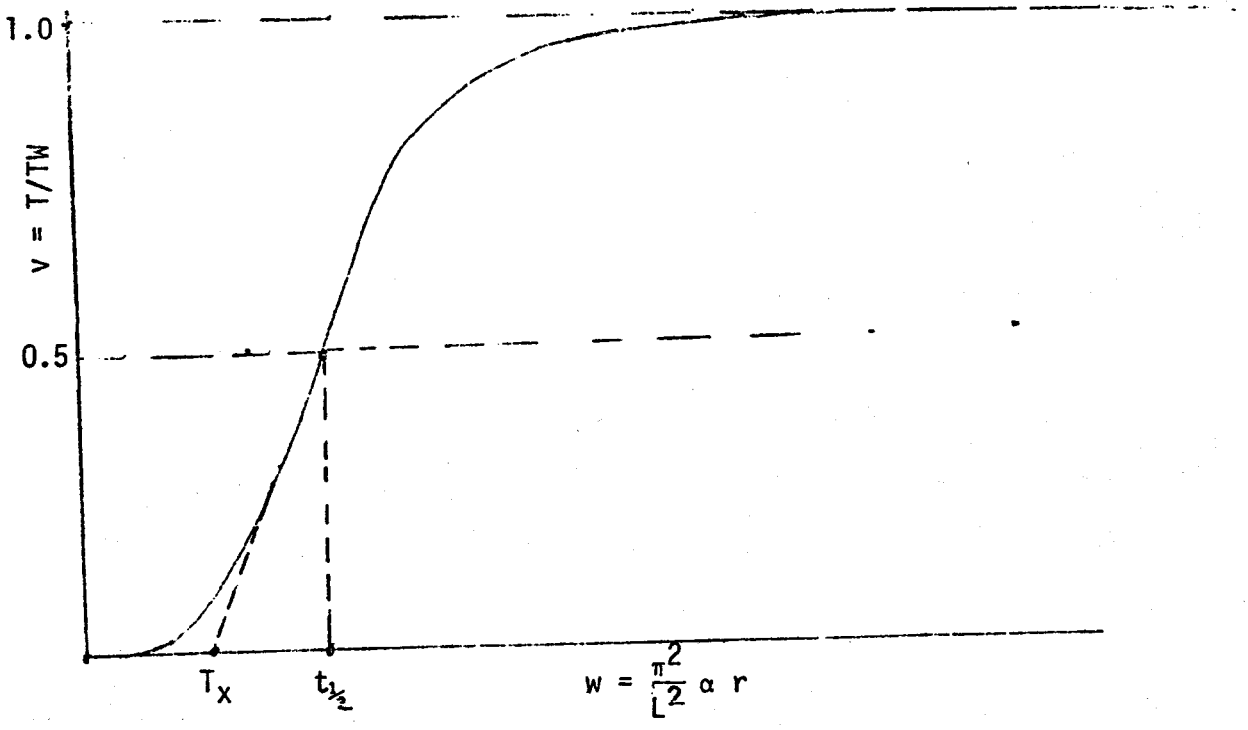

from equation (1). At V = .5 $\alpha = (1.38\ L^2/\pi^2\ t_{\frac{1}{2}})$ or (2)

at time axis intercept (t_x) of the interpolated straight line portion of Figure 1,

$$t_x = 0.48\ W \quad \text{or} \quad \alpha = (0.48\ L^2/\pi^2\ tx) \tag{3}$$

equation 3, yields more accurate diffusivity values than equation 2 (Parker, 1959, Jenkins, 1961).

Thermal conductivity can be calculated from α by the following relation $k = \alpha\ PC$, where k is thermal conductivity and PC is the thermal heat capacity of the saturated rock. The thermal heat capacity of water saturated rock is given by:

$$PC = P_s\ C_s\ (1-\phi) + \phi\ P_w\ C_w \tag{4}$$

where subscript s denotes solid and w denotes water and ϕ is porosity. To estimate the heat capacity of a water saturated sample, the specific heats (C), and densities (P) of both water and solid, and the porosity must be known.

The determination of thermal conductivity requires measuring both the thermal diffusivity and heat capacity. The thermal diffusivity is measured using the flash technique as described above. Single, short (5 m sec.), and intense pulses of infrared are utilized for heating the front face of samples. Samples are disc shaped, 3 mm thick and 2.0 cm in diameter. Their front faces are coated with a thin coat of camphor black for maximum and uniform absorption of incident energy. Figure 2 shows a pictorial diagram of the thermal diffusivity equipment.

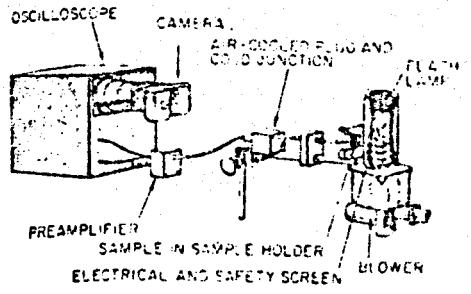

Pictorial schematic of test setup.

The heat capacity of water saturated samples is calculated from equation 5. Heat capacity of water at different temperatures and pressures is calculated from available tables. Heat capacity of dry rock samples is estimated using calorimetric methods on samples which were employed for electrical conductivity measurements.

RESULTS

A sample of the measurement results follows.

Sample Transient Measurement

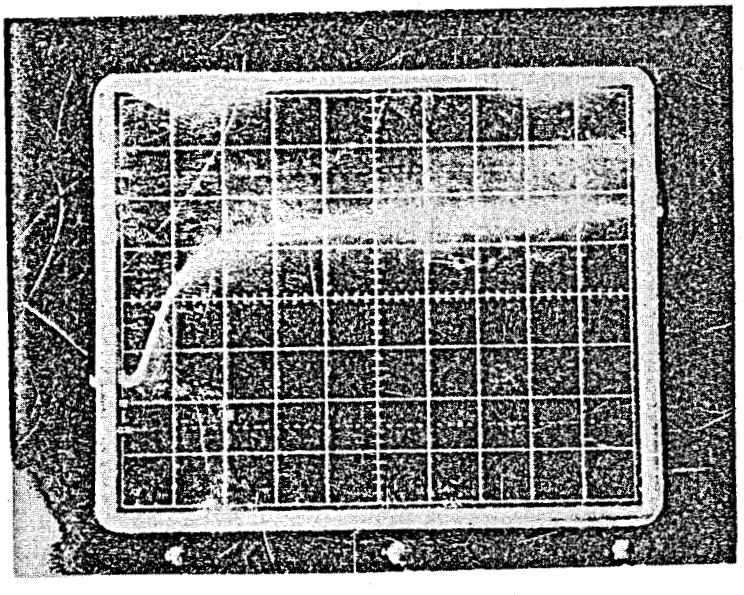

$t_{\frac{1}{2}}$ = 1.85 seconds

Temp. = 55°C

CAPILLARY PRESSURE MEASUREMENTS

Most rock properties depend upon the pore structure of the rock, that is pore geometry, volume, size, and distribution. Because of the influence of pore structure on rock resistivities and seismic velocities, measurements of capillary pressure curves -- one of the more direct ways to characterize pore structure -- were undertaken.

BACKGROUND AND THEORY

Capillary pressure measurements involve two physical phenomena--surface tension and wettability.

When two immiscible fluids such as hydrocarbons and water in a pore system are placed in contact, the surface of contact is almost always curved. This results from the fact that the molecules of one of the fluids will normally have a greater inter-attraction for each other than intra-attraction for the molecules of the other fluid across the contact area. As a result the fluid where the intermolecule attraction is greater than the intramolecule attraction tends to draw up into a sphere, causing a curved surface of separation between the fluids.

A curved surface between the fluids can only be maintained if there is a net force across the fluid interface with an attendant net pressure across the interface. It is this pressure which is defined to be "capillary pressure" for the immiscible fluid system. Thus the capillary pressure turns out to be the pressure discontinuity across the interface separating immiscible fluids.

The magnitude of the capillary pressure, P_c, is given by Plateau's equation

$$Pc = \alpha \left(\frac{1}{R_1} + \frac{1}{R_2}\right)$$

where α is the "surface tension" of the two fluids and R_1, R_2 are the principal radii of curvature of the contact surface between the fluids. Thus Plateau's equation predicts that the pressure change across the interface is a function of the geometry of the interface (as expressed by the radii of curvature of the surface) and the relative inter- and intra-molecular attractions of the two types of fluid molecules (accounted for mathematically by the surface tension, α).

If the contact surface happens to be spherical (as they tend to be), Plateau's equation then becomes

$$Pc = 2\,\alpha/R$$

where R is the radius of the sphere.

Wherever the immiscible fluid contact surface encounters a solid (such as at a pore wall in the pore system of a rock, the angle between the tangent to the immiscible fluid contact surface and the solid surface <u>at the point of contact</u> is a constant (Θ in Figure 4). This is a reflection of the fact that in general the molecules of the solid have a greater intra-attraction for the molecules of one of the fluids relative to the intra-attraction of the solid for the molecules of the other fluid. Thus there is a tendency for one of the fluids to displace the other fluid from the solid surface, a phenomenon called "wettability". The angle Θ provides a measure of the wettability of one fluid relative to the other for the solid. When measured through either one of the fluids, if it is less than 90^{o}, that fluid is said to be the wetting fluid; if it is greater than 90^{o}, that fluid is said to be non-wetting. Thus the term "wettability" is a relative one. It is an indication of how much more one fluid tends to "wet" the solid surface than the

DIST. OF IMMISCIBLE FLUID IN POR CHANNEL

EQUIL. FOR LOWER P_c

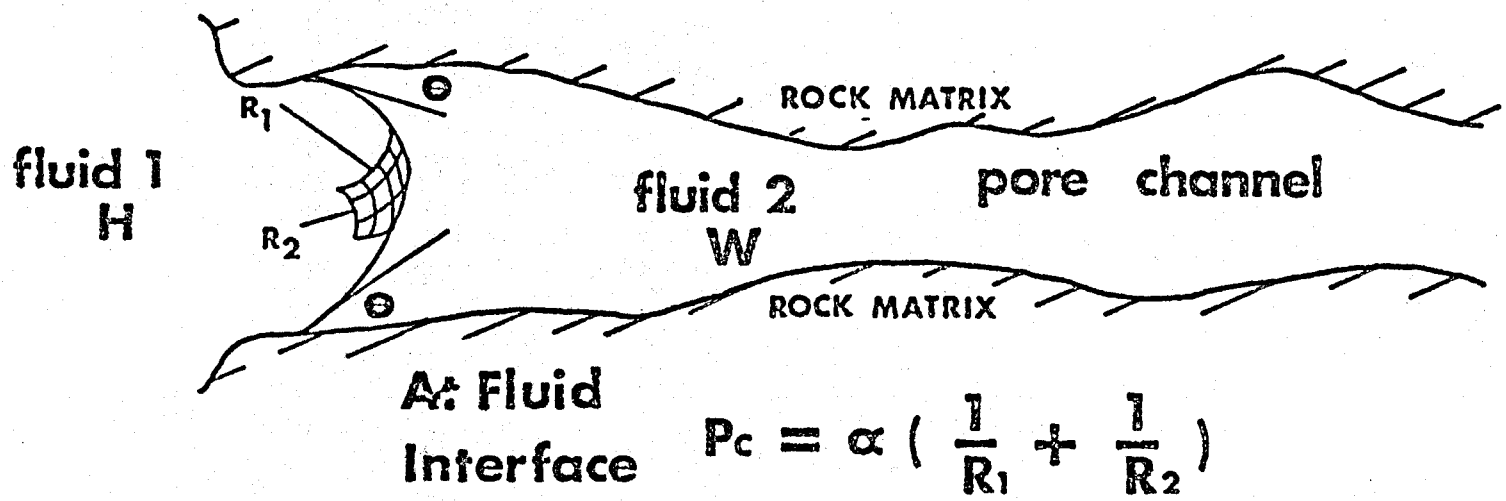

(a) lower P_c

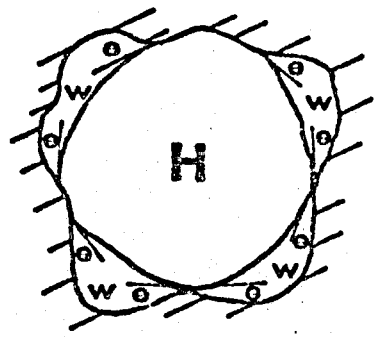

EQUIL. FOR HIGHER P_c

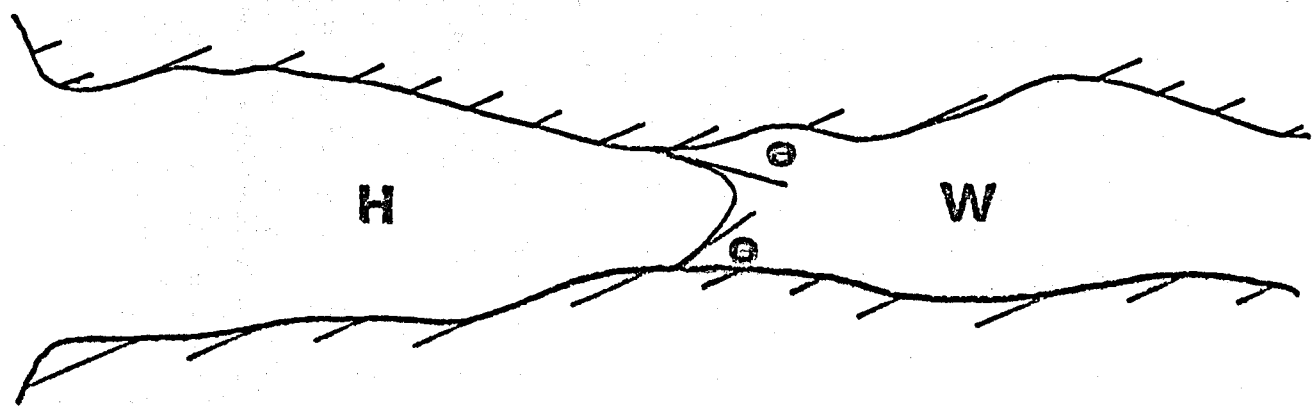

(b) higher P_c

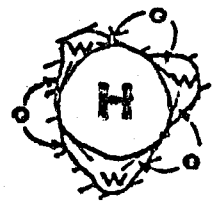

FIGURE 4

other fluid. It is a characterization of the relative molecular attractions of the three or more materials (solid and two or more immiscible fluids) involved.

Distribution of Immiscible Fluids in Pore Systems

The available evidence indicates that in petroleum reservoirs, water tends to be the wetting fluid and hydrocarbons tend to be the non-wetting fluid for the rock surfaces such as pore walls.

Consider now what happens when introduction of a non-wetting phase (hydrocarbon, H in Figure 4A) into an initially wetting fluid (water, W in Figure 4A) saturated pore system is attempted. The hydrocarbon water interface cannot enter the pore system until the interface is sufficiently curved to accomodate to the largest pore openings available (i.e., the radii of curvature in Plateau's equation for Pc must be equal to or less than the dimensions of the pore openings). This requires, in turn, a sufficient capillary pressure (Pc) given by Plateau's equation. The threshold capillary pressure (Pc) required to achieve entry of the non-wetting phase into the pore system is called "displacement pressure" and represented by the symbol Pd.

Pore channels are normally irregular in shape. Once the non-wetting/wetting fluid interface is inside such a pore channel it will migrate to the first equilibrium position where Plateau's Equation can be satisfied at the non-wetting/wetting fluid contact and at the same time the contact angle Θ can be maintained wherever the fluid interface contacts the pore walls.

The available capillary pressure (Pc) and the surface tension determine the curvature of the fluid interface. The contact angle Θ for the

particular combination of rock and fluids and the geometry of the pore channel then determine where the fluid contact curvature can be accomodated. The position of the immiscible fluid interfaces within the various pore channels comprising the rock's pore system determine the relative amounts of water and hydrocarbons within the rock (the saturations). Thus a combination of pore geometry, wettability (Θ), fluid surface tension (α) and capillary pressure (Pc) controls the water saturation in the rock. If the capillary pressure is changed, the fluid interfaces must migrate to new equilibrium positions (Figure 2B) within the pore channels where the new interfacial curvatures and Θ can be accomodated, thus changing the saturations of the component fluids.

Capillary Pressure Curves

These concepts led to the idea of making capillary pressure measurements on cores. Usually in these experiments (Figure 5) the core sample is initially at a wetting fluid saturation of 100%. Any combination of fluids can be used as long as one is a relatively wetting fluid and one is a relatively non-wetting fluid. For example, mercury-air is a commonly used and experimentally convenient combination, the air acting as a wetting fluid and the mercury as a non-wetting fluid.

When the injection capillary pressure experiment starts, the non-wetting fluid completely surrounds the exterior of the rock sample. Normally (unless gravity drainage occurs through very large openings), the non-wetting fluid does not enter the pore system until the external pressure Pc is large enough to bend the wetting/non-wetting fluid interface into a radius of curvature small enough to fit through the largest pore openings available on the surface of the rock.

CAP PRESSURE EXPERIMENT (INJECTION)

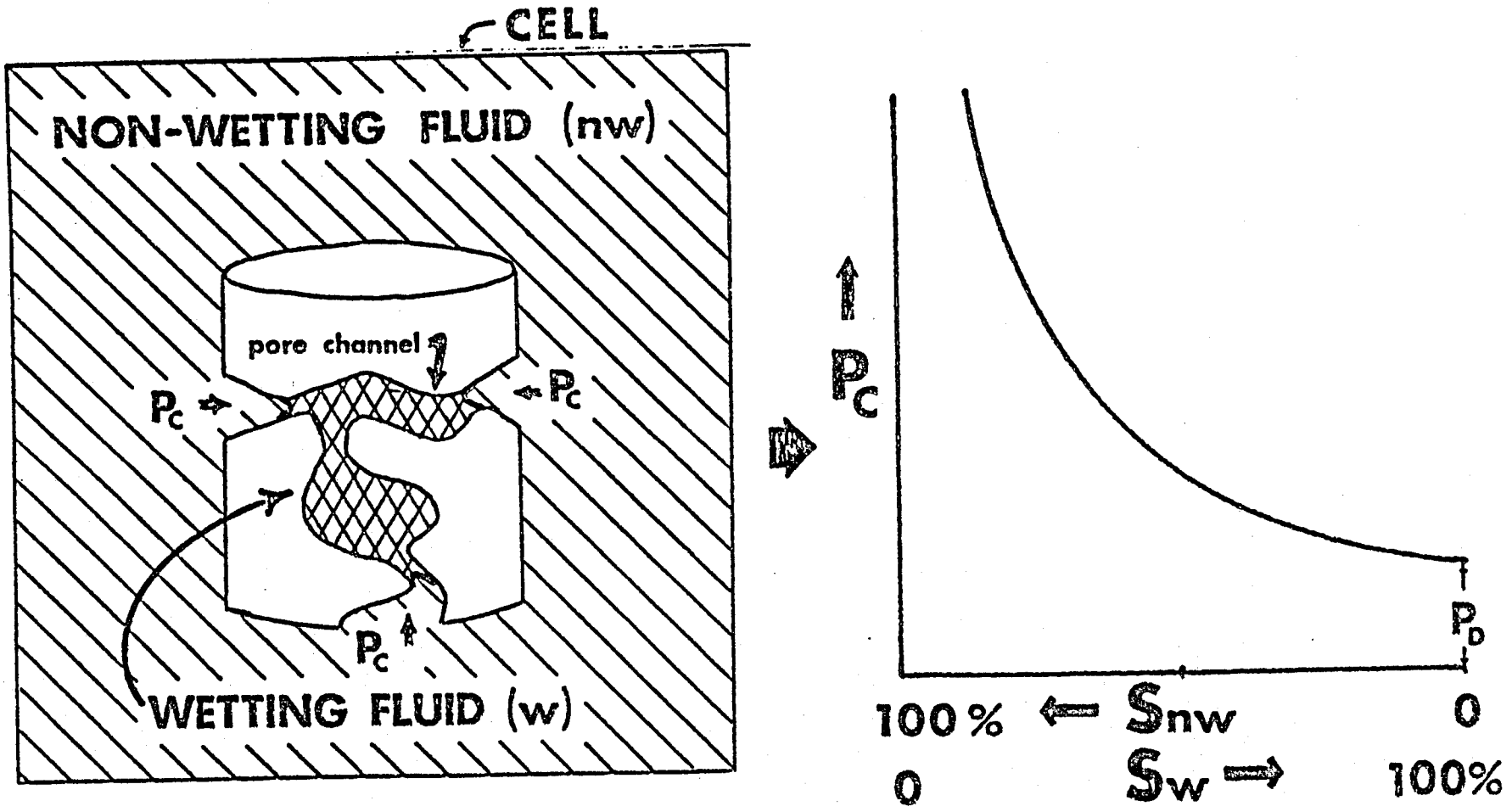

FIGURE 5

Once Pc exceeds this "displacement pressure", fingers of non-wetting fluid enter the pore channels of the rock and in each pore channel entered, progress to the first point where, for the Pc applied, Plateau's equation can be satisfied at the fluid interface and the contact angle θ maintained at the pore wall. For the non-wetting fluid to proceed past this point as a continuous phase enough pressure must be applied to the non-wetting phase to force the fluid interface into a configuration with small enough radii of curvature to pass further into the pore channel. The fluid interface will then move to the next place in the pore channel where Plateau's equation can be satisfied for the new pressure (Pc) and the contact angle (θ) maintained at the pore wall surfaces. As the pressure Pc is increased, the curvature of the wetting/non-wetting fluid interface increases and the fingers of non-wetting fluid can penetrate into smaller and smaller pore channels as they seek new equilibrium positions. If a "bottleneck" (constriction in the pore channel between two larger pore openings) is encountered, beads of non-wetting fluid will break off to fall into any larger pore space beyond the bottleneck until the Pc is large enough for the non-wetting fluid to pass the bottleneck as a continuous phase.

Typically from this experiment we get a curve such as that on the right side of Figure 6. Generally, as the pressure needed to inject non-wetting fluid increases, the fluid is entering pore channels with smaller and smaller cross section areas. Therfore the curve is often interpreted as a pore-size distribution curve, the magnitude of Pc being a measure of pore size, the increment of Sw for a given Pc being a measure of the portion of the total porosity consisting of that pore size.

CAP CURVES AND S_W PROFILES

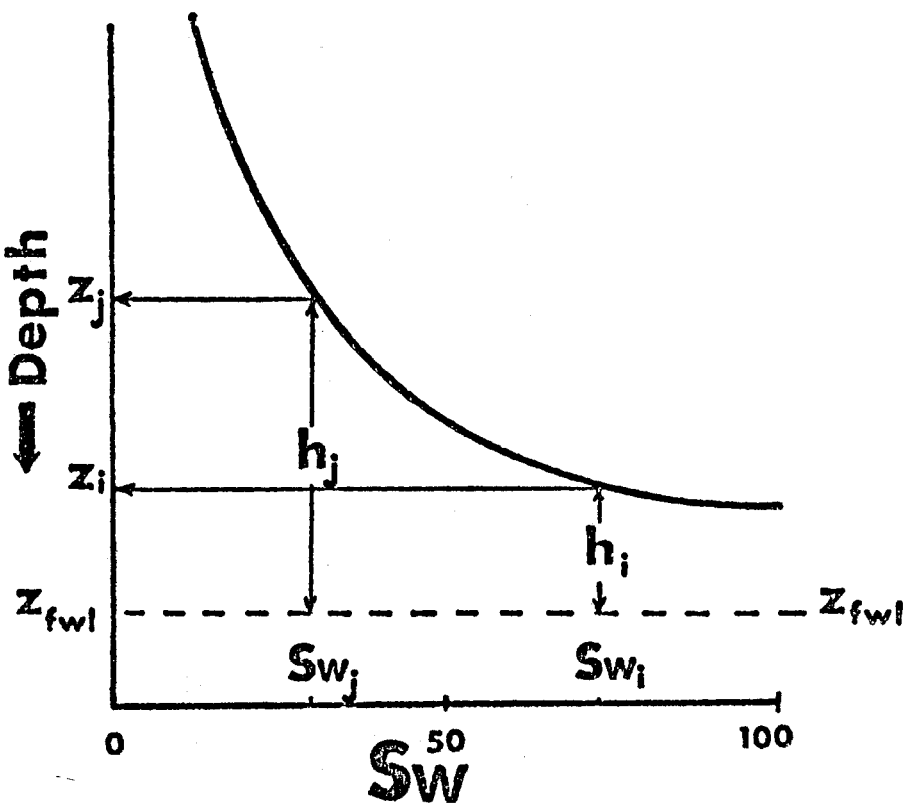

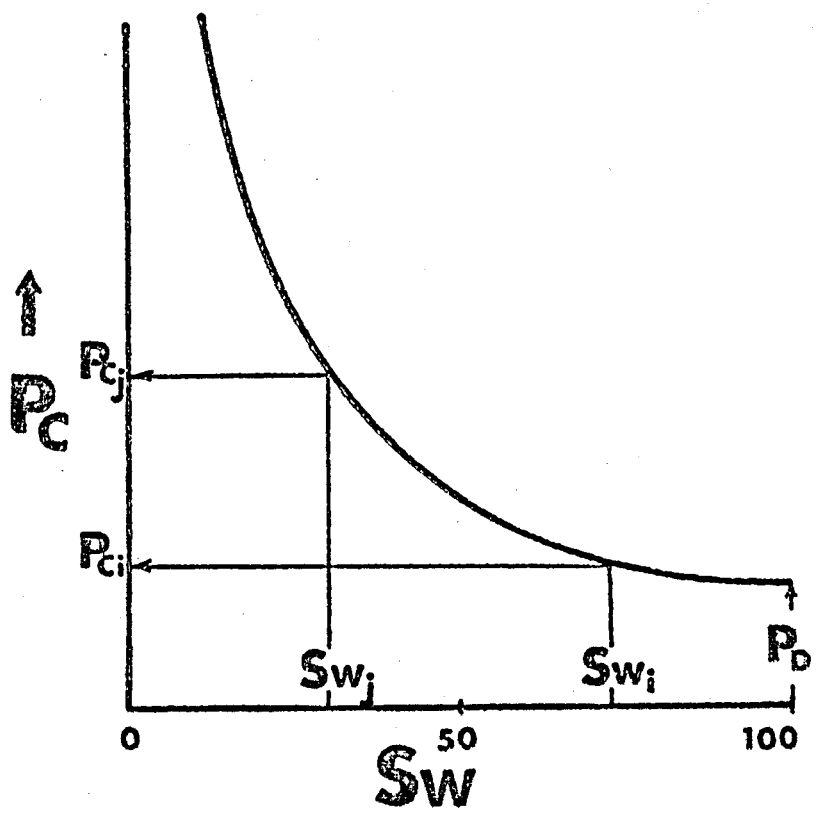

$$Pc_i = Ch_i \quad \text{or} \quad Pc_i = C Z_{fwl} - C Z_i$$

FIGURE 6

However, it should be remembered that the curve must also reflect the number, distribution and sizes of the bottlenecks or constrictions between larger pore openings.

Hysteresis Measurements, Initial-Residual Curves and Prediction of Water Drive Recoveries

The question naturally arises as to what will happen, if after injection of non-wetting fluid in the capillary pressure experiment, the pressure Pc is now reduced. When this happens, of course, the non-wetting fluid tries to flow back out of the pore system, or, more correctly, the wetting fluid tries to drive the non-wetting fluid back out of the pore system.

If Pc is reduced, the non-wetting fluid will fully withdraw from the pore system until Pc becomes smaller than the pressure necessary to support a continuous non-wetting fluid phase at the smallest pore bottleneck (constriction) that has been passed in the injection process. At this point, the continuous non-wetting fluid finger is broken, and some non-wetting fluid is trapped in the pore system behind this constriction. The non-wetting fluid can then be withdrawn until the pressure becomes insufficient to support a continuous phase at the next larger constriction, when again the non-wetting fluid finger is broken and some more non-wetting fluid is left in the pore system. Thus, when Pc is finally reduced to zero, non-wetting fluid will be left trapped in various parts of the pore system. This results in a "hysteresis" capillary pressure curve. The amount of non-wetting fluid left trapped in the pore system will increase with increasing injection pressure Pc reached, since smaller and smaller constrictions are passed with higher and higher Pc's. Thus, if we were to carry out the hysteresis

experiment to several different and increasing Pc's, we would expect to obtain curves something like those in Figure 7.

When we withdraw the non-wetting fluid from the pore system by reducing Pc, we are simulating the displacement of a non-wetting fluid by a wetting fluid. Thus the amount of non-wetting fluid left in the pore system is a measure of the residual non-wetting fluid for the initial saturation reached at the particular Pc used on the injection experiment.

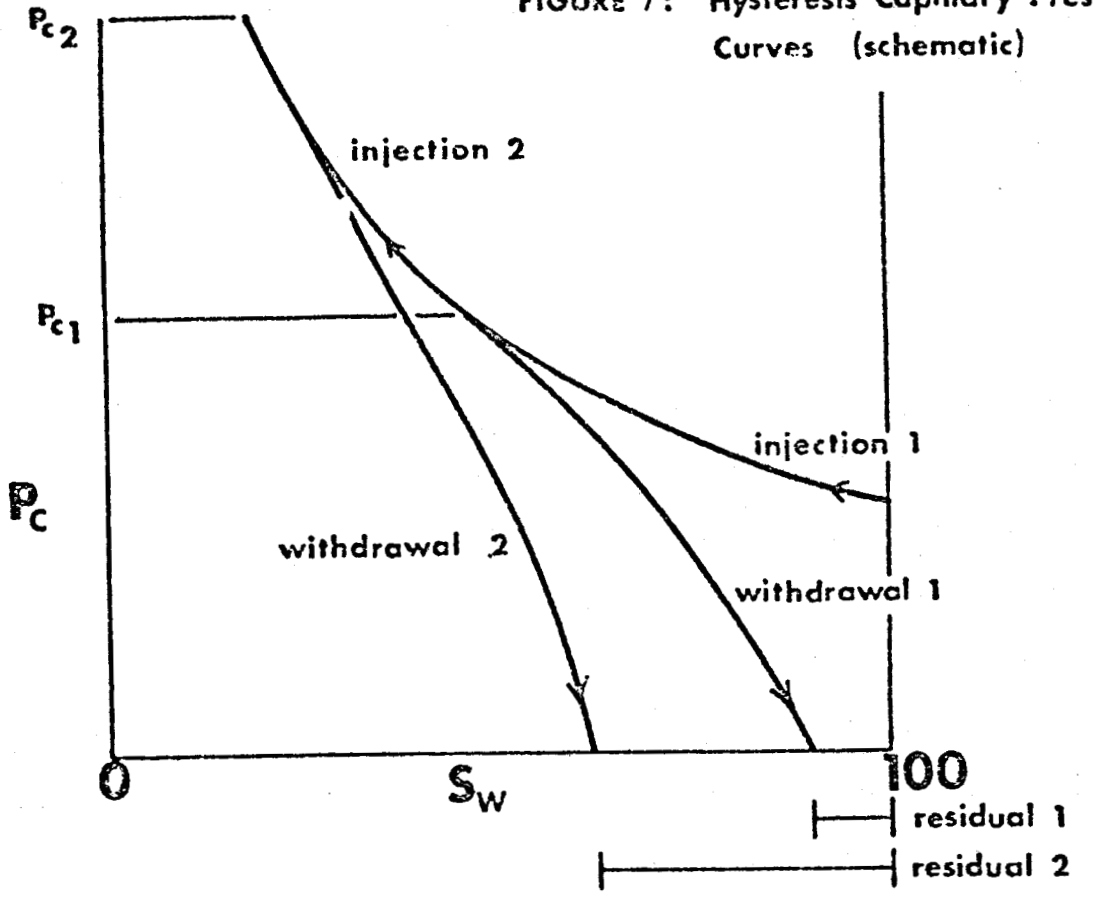

FIGURE 7: Hysteresis Capillary Pressure Curves (schematic)

MEASUREMENTS

The mercury injection technique was chosen to measure capillary pressure curves because 1) the measurements are quicker than other techniques and 2) the pressure available is greater than in other methods.

Measurements of capillary pressure curves were made with a Model 1057 Ruska Mercury-Injection capillary pressure apparatus. Before measurements could begin both the samples and the apparatus were prepared. The samples must be less than 2.5 cm in diameter and 3.75 cm long. After samples were cut to the proper size they must be completely dried. The measuring apparatus must then be cleaned to remove old traces of mercury and calibrated. The sample is then placed in a pycnometer and the system is evacuated. Mercury is then injected to file the system and the bulk volume of the core is calculated. Nitrogen is next forced into the system and additional mercury is again injected to refill the system. The volume of mercury injected under various pressures combined with calibration information results in a capillary pressure curve.

Figures 8 through 28 show capillary pressure curves for numerous samples. The porosity abscissa is a measurement of the fractional porosity as a function of the porosity calculated in an earlier phase of this project. For example, in Figure 28 for sample C-2-41 the total porosity previously calculated was 15%. About 50% of this porosity was injected with mercury at higher pressures. The black line (x) to the left indicates the loading of injection capillary pressure curve while the red line (t) to the right shows the withdrawal curve.

Interpretation

From the basic capillary pressure curves and hysteresis curve, interpretations of pore size, pore structure, and permability can be made.

Figures 29 through 44 show pore size distributions for 16 of the samples tested. The abscissa shows the pore entry radius in cm and the ordinate charts distribution as cm^{-1}. The distribution numbers indicate the area under the curve; the total area is normalized to one. These curves may be viewed as histograms to easily understand pore size distribution. The equation used to calculate pore size distribution is:

$$D(\gamma_i) = \frac{P_{ci}}{r_i} \frac{dS_m}{dP_c} \qquad \text{(Purcell, 1949)}$$

where P_{ci} is capillary pressure

r_i is pore entry radius

and S_m is mercury saturation as a percentage of pore volume.

Permeability can also be calculated directly from the capillary pressure curves:

$$K = 1.426 \times 10^4 \phi\lambda \int_{S=0}^{S=1} \frac{ds}{(P_c)^2} \qquad \text{(Purcell, 1949)}$$

K is permability

ϕ is porosity

λ is a lithology factor dependent upon mercury contact angle and surface tension. For the curves the number 0.216/psi has been used.

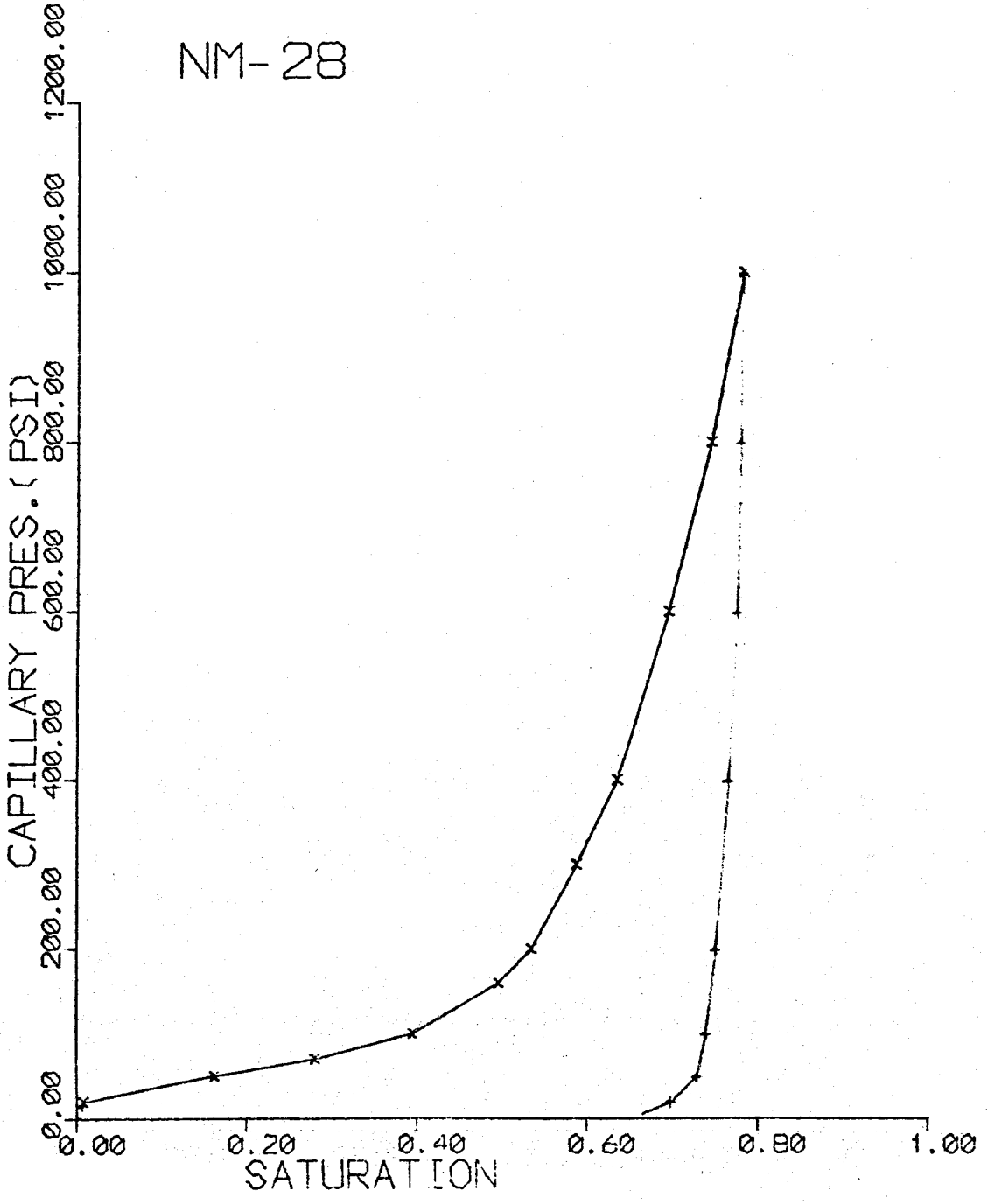

Figure 8

Experimental Capillary Pressure Curve for Sample NM-28

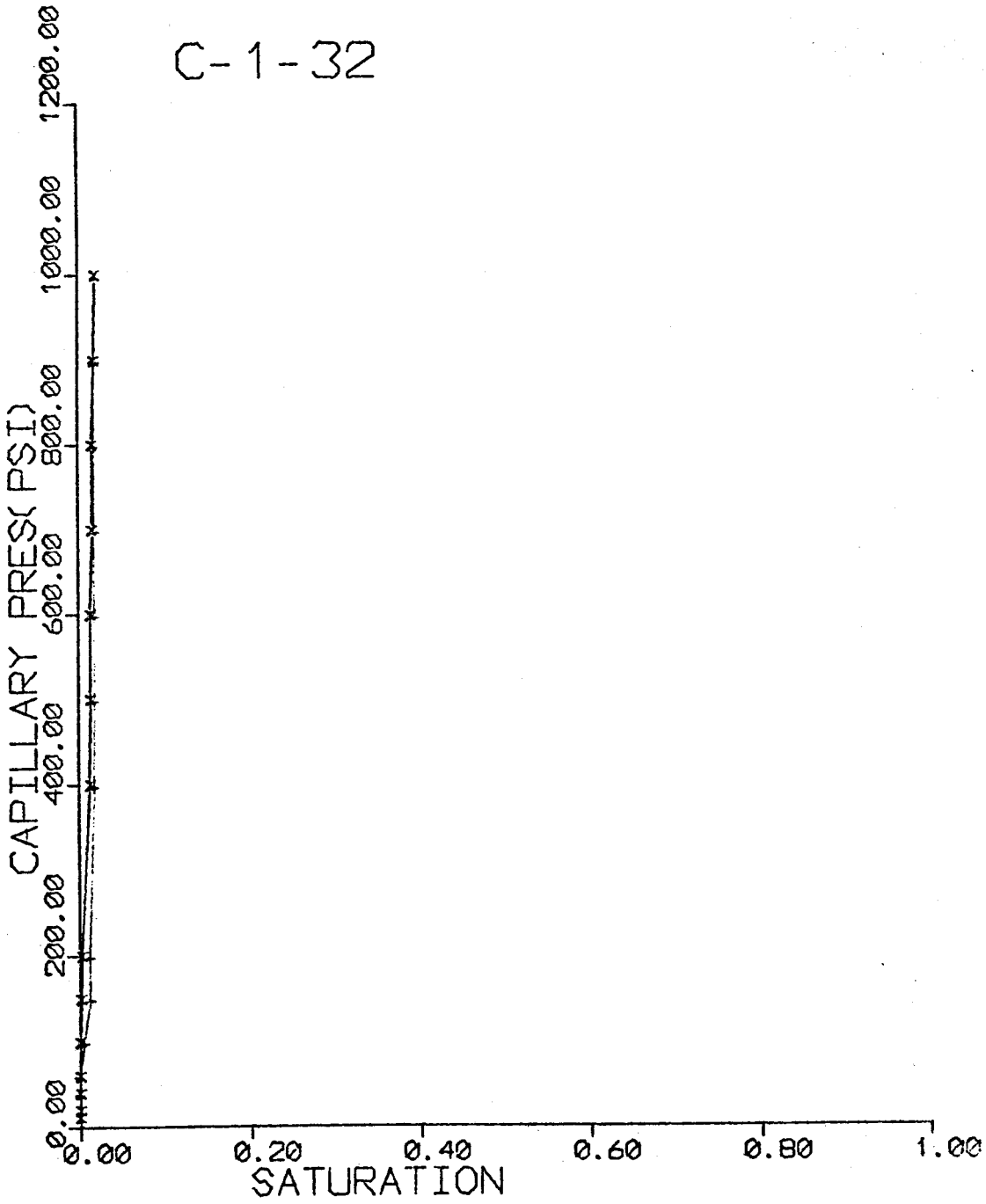

Figure 9

Experimental Capillary Pressure Curve for Sample C-1-32

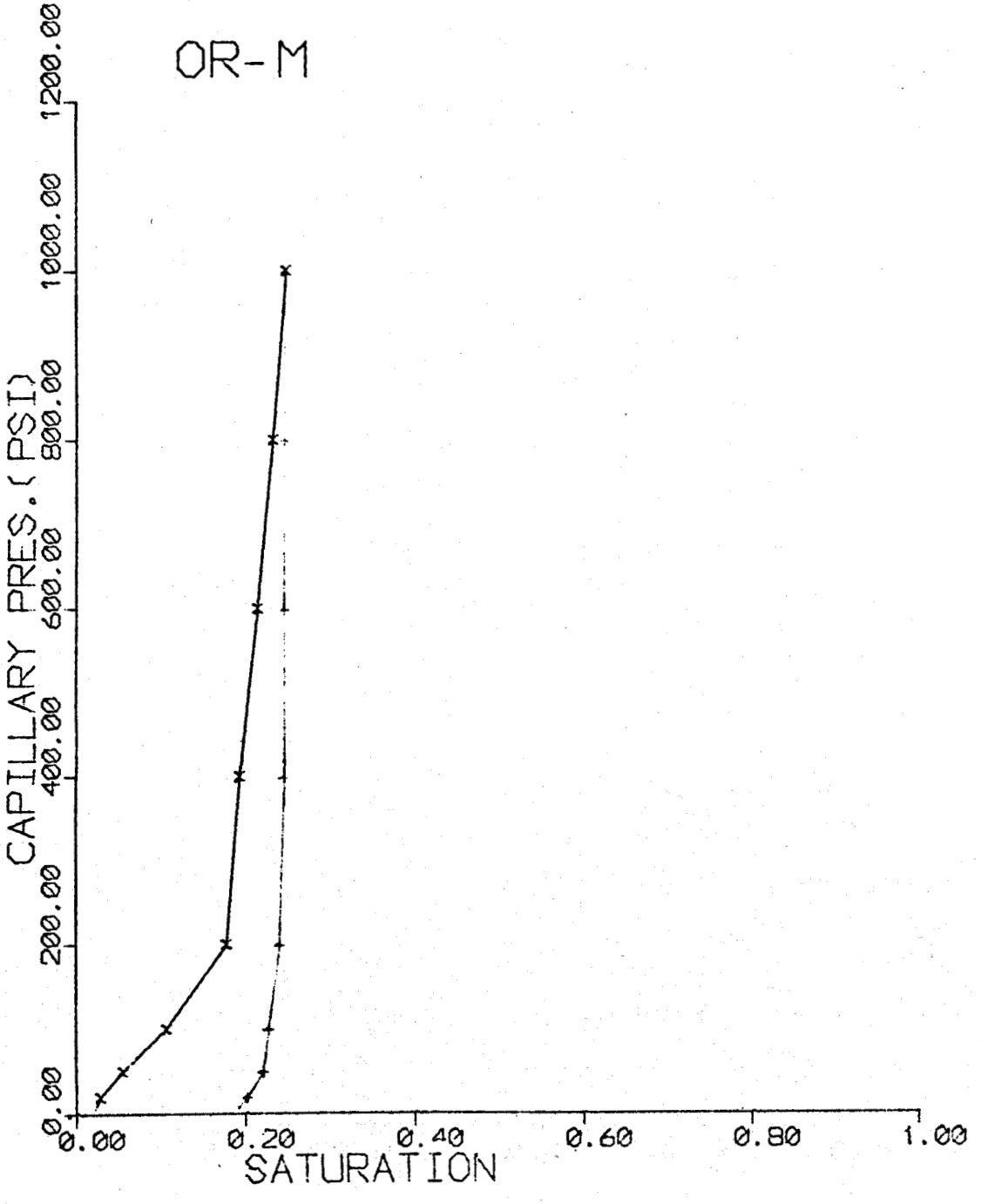

Figure 10

Experimental Capillary Pressure Curve for Sample OR-M

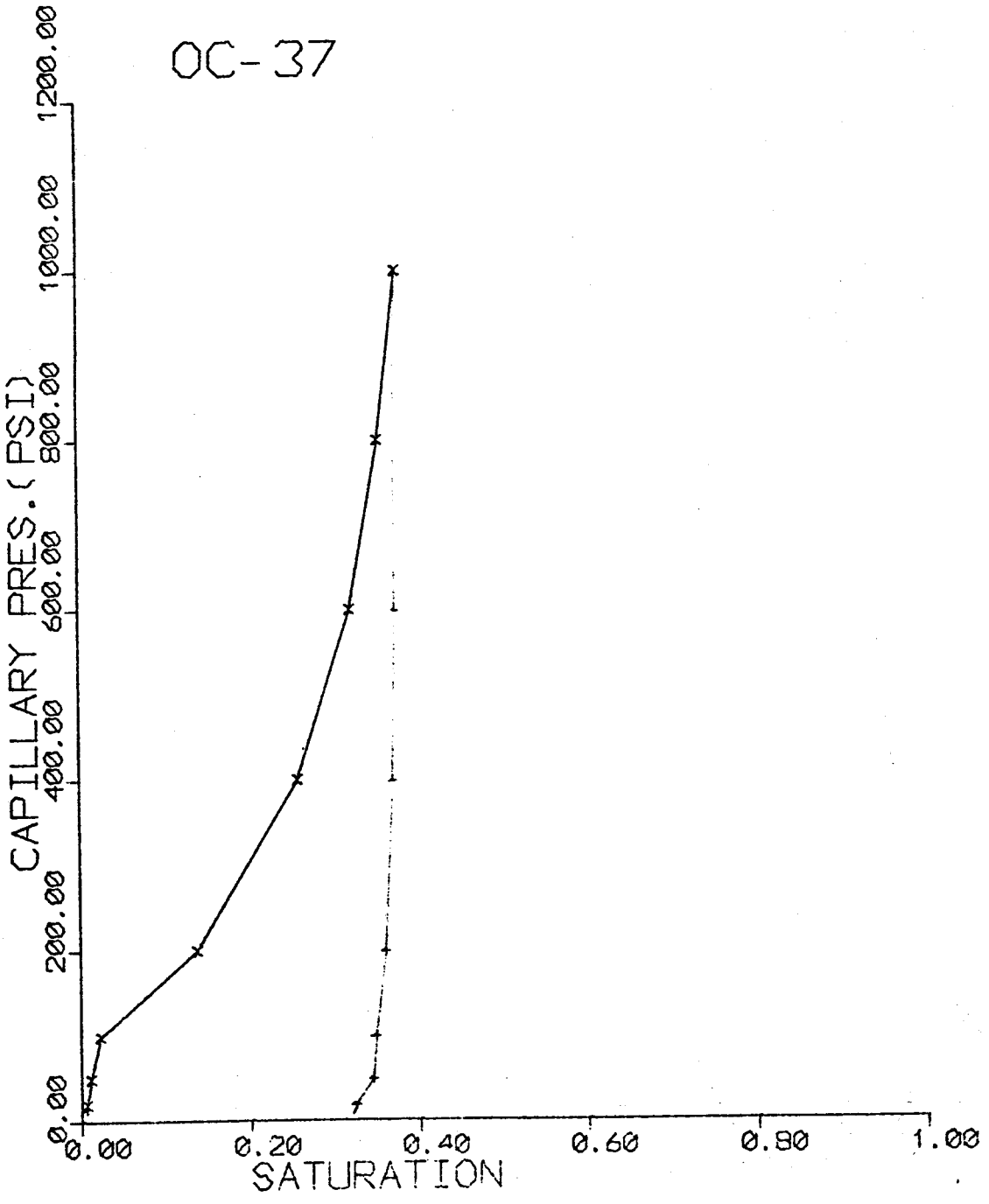

Figure 11

Experimental Capillary Pressure Curve for Sample OC-37

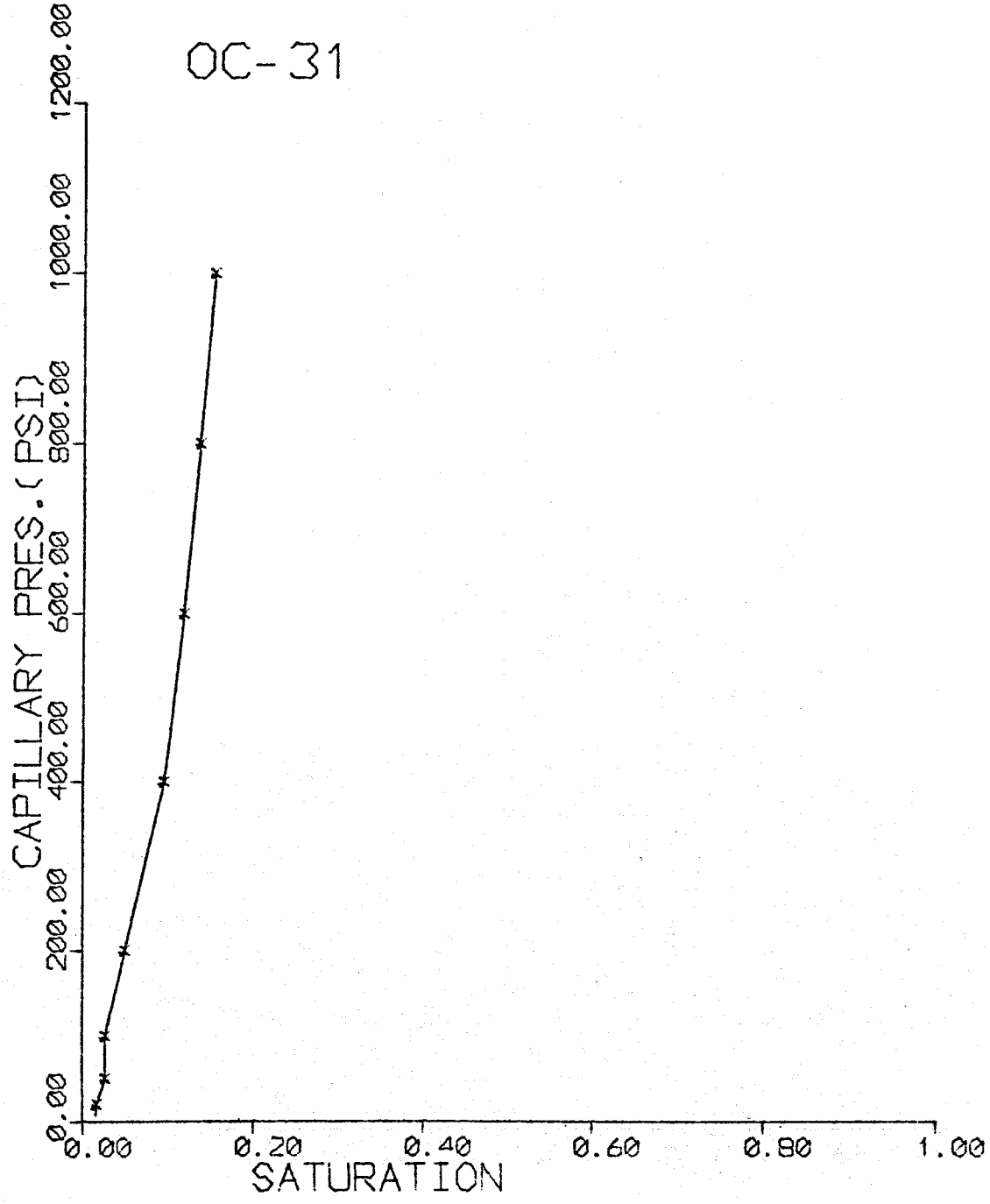

Figure 12

Experimental Capillary Pressure Curve for Sample OC-31

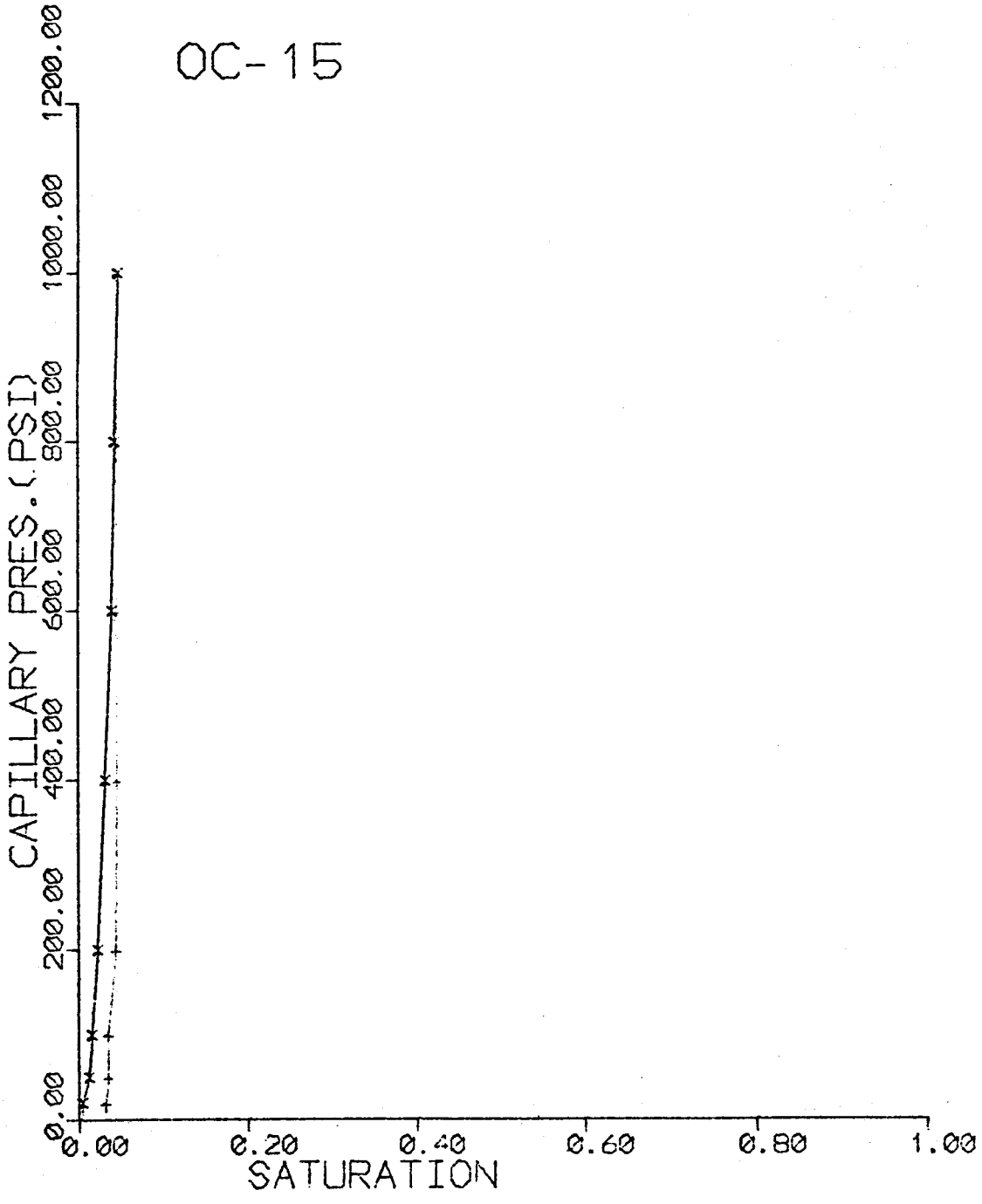

Figure 13

Experimental Capillary Pressure Curve for Sample OC-15

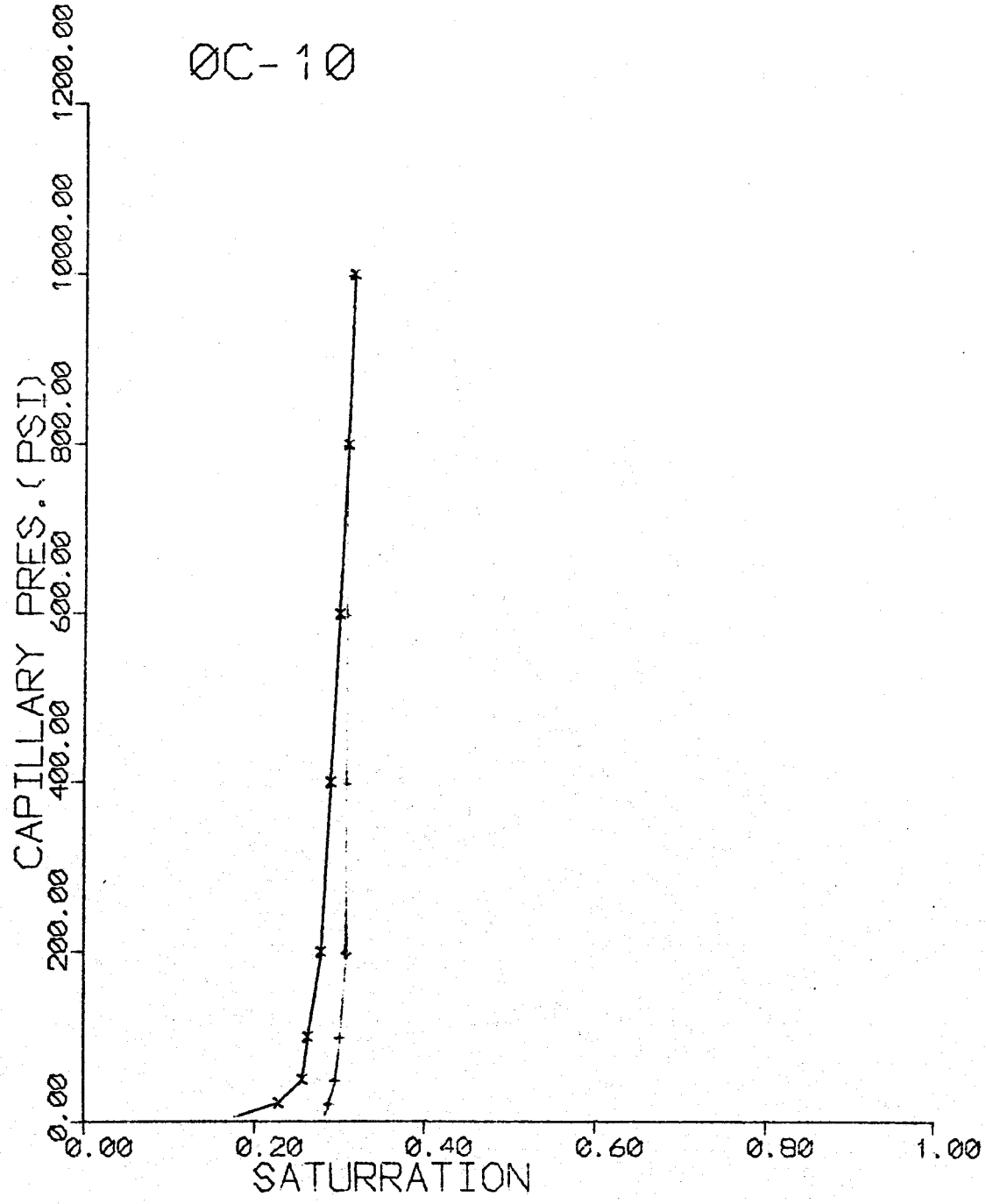

Figure 14

Experimental Capillary Pressure Curve for Sample ØC-10

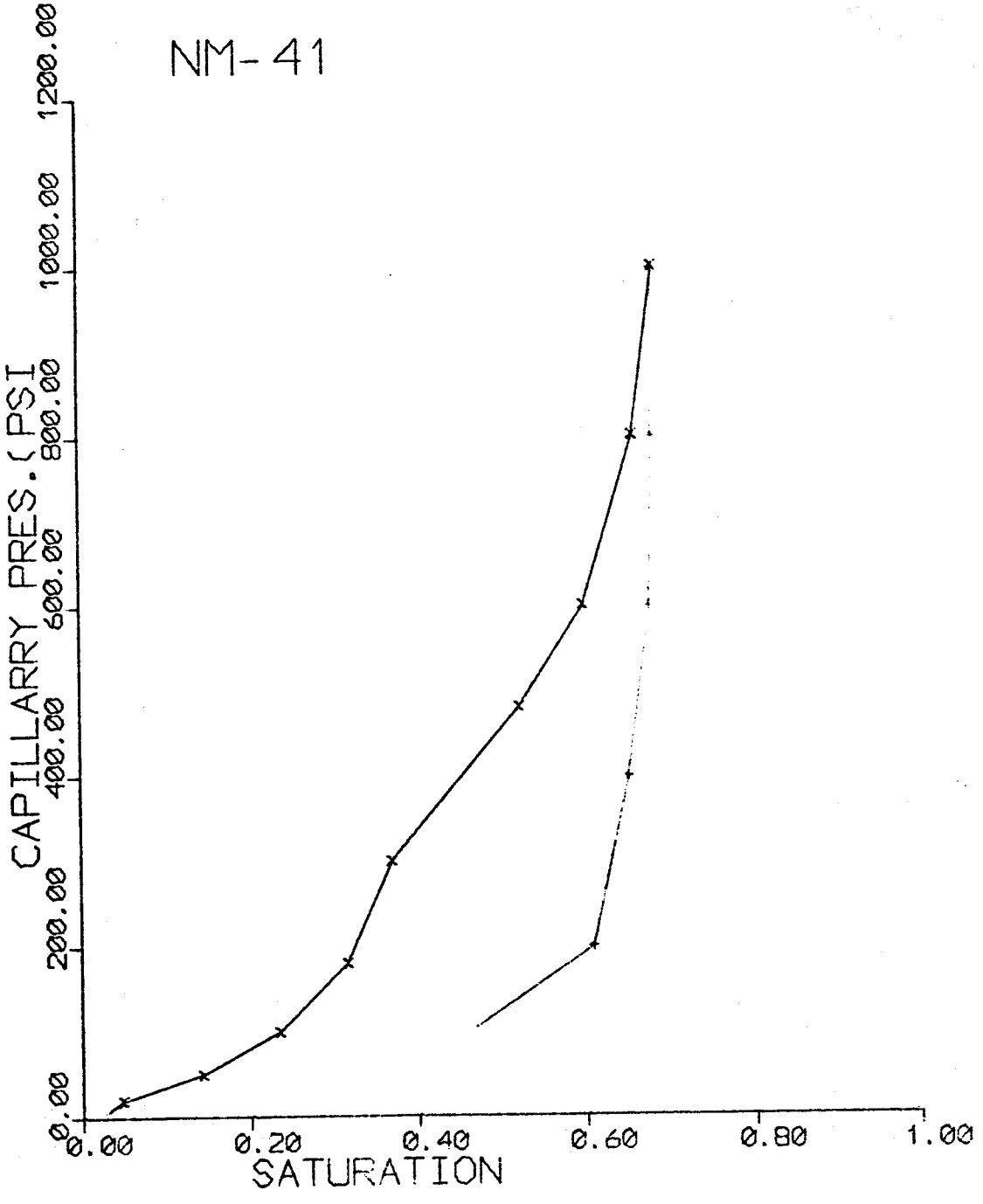

Figure 15

Experimental Capillary Pressure Curve for Sample NM-41

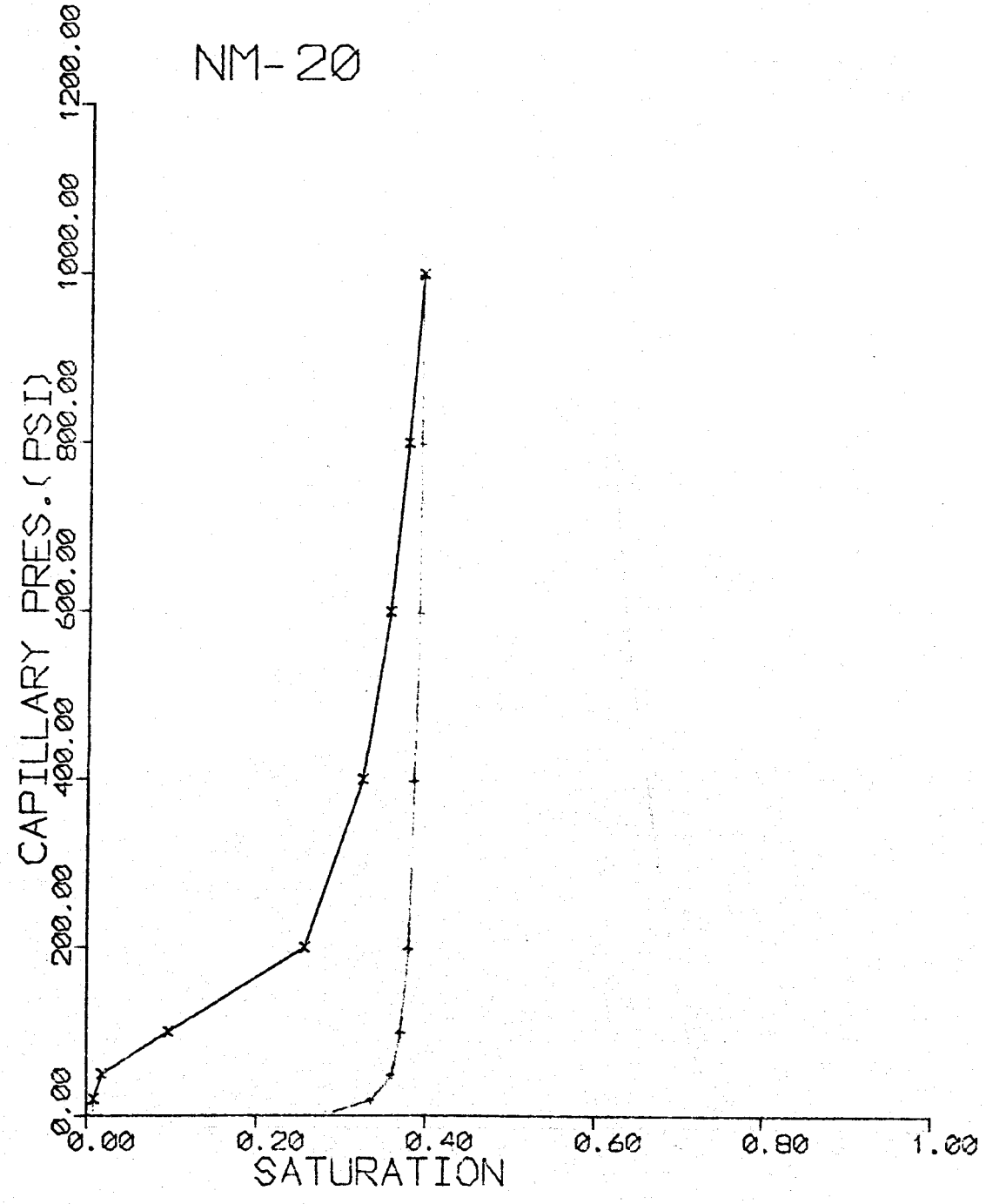

Figure 16

Experimental Capillary Pressure Curve for Sample NM-20

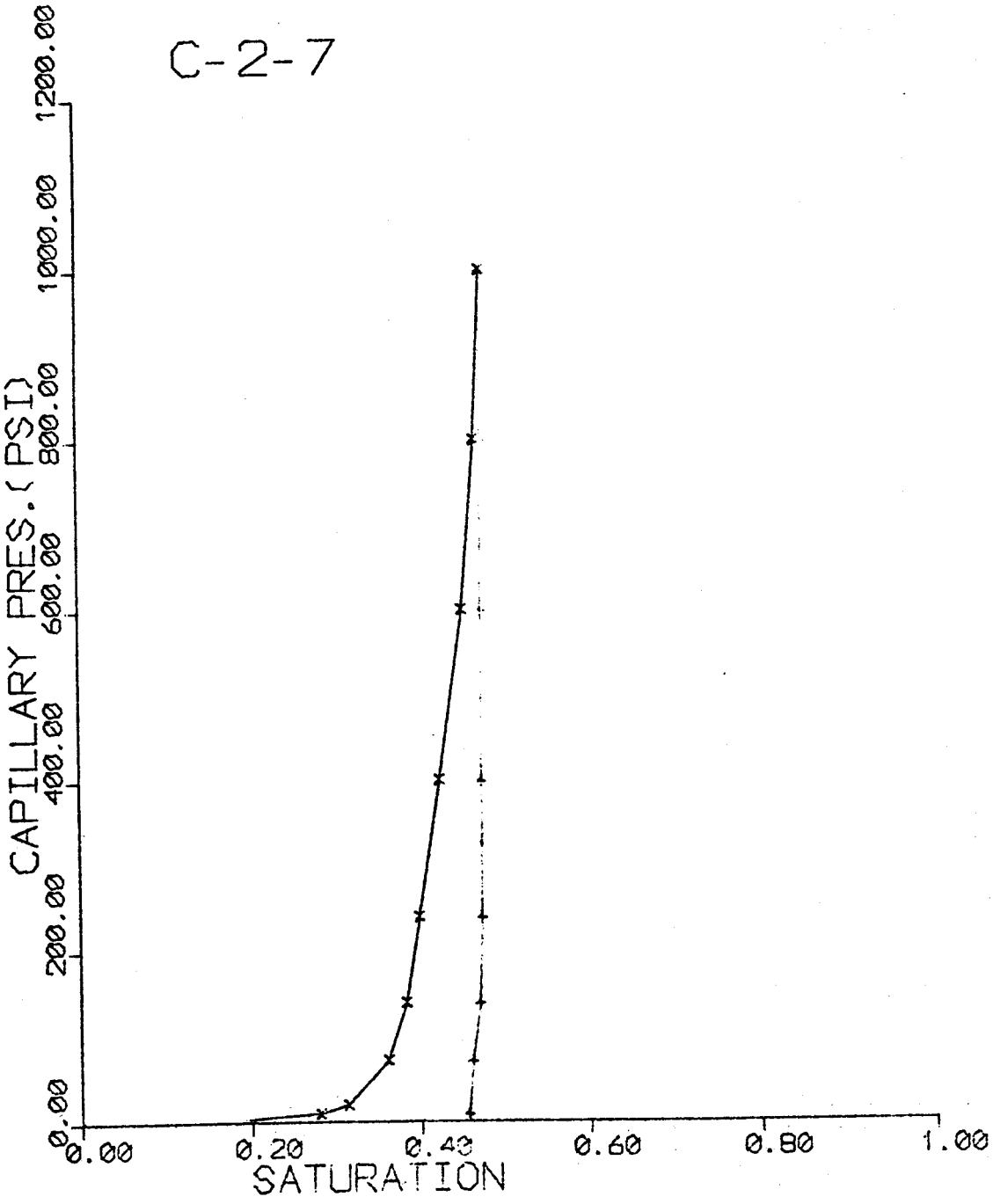

Figure 17

Experimental Capillary Pressure Curve for Sample C-2-7

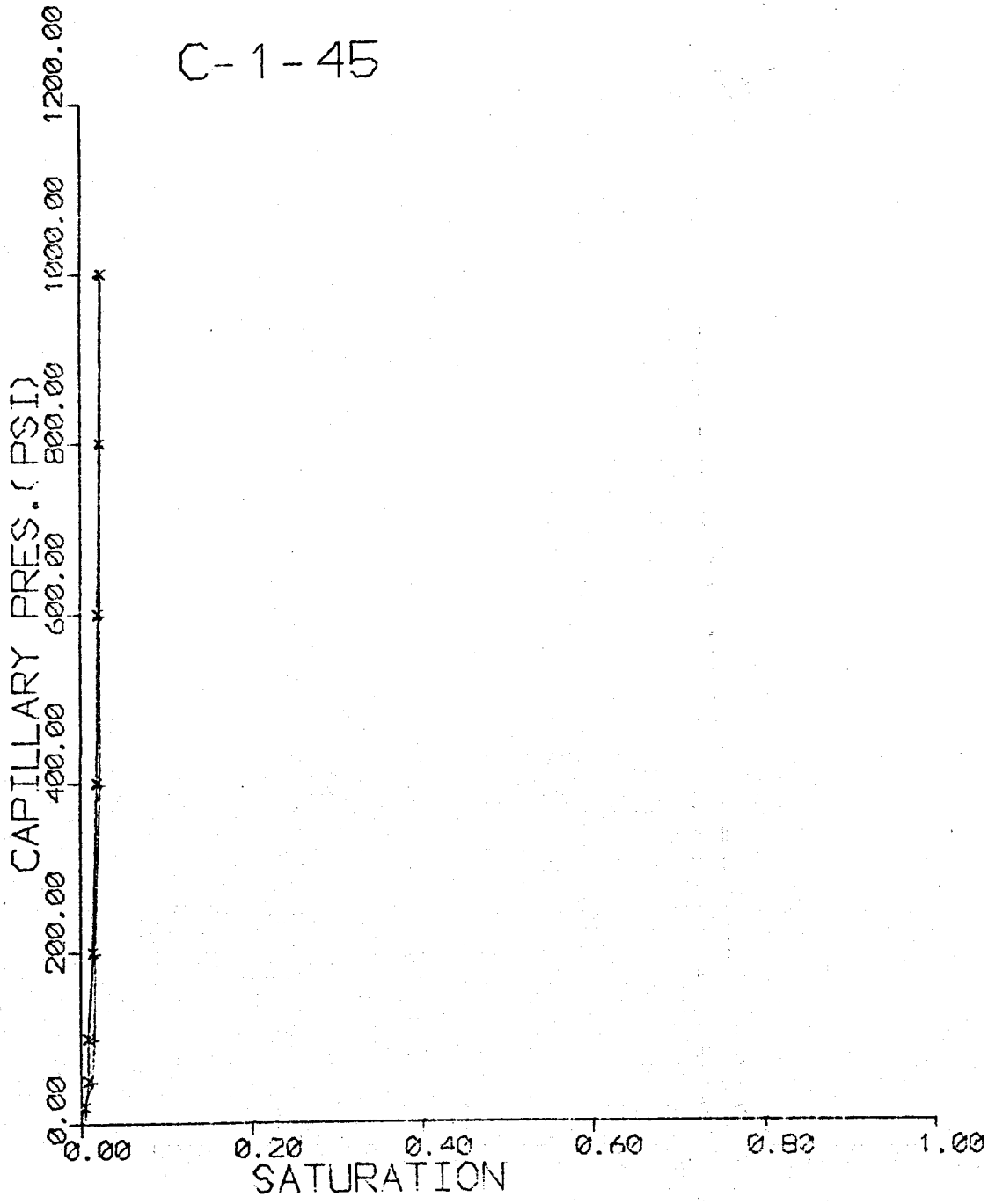

Figure 18

Experimental Capillary Pressure Curve for Sample C-1-45

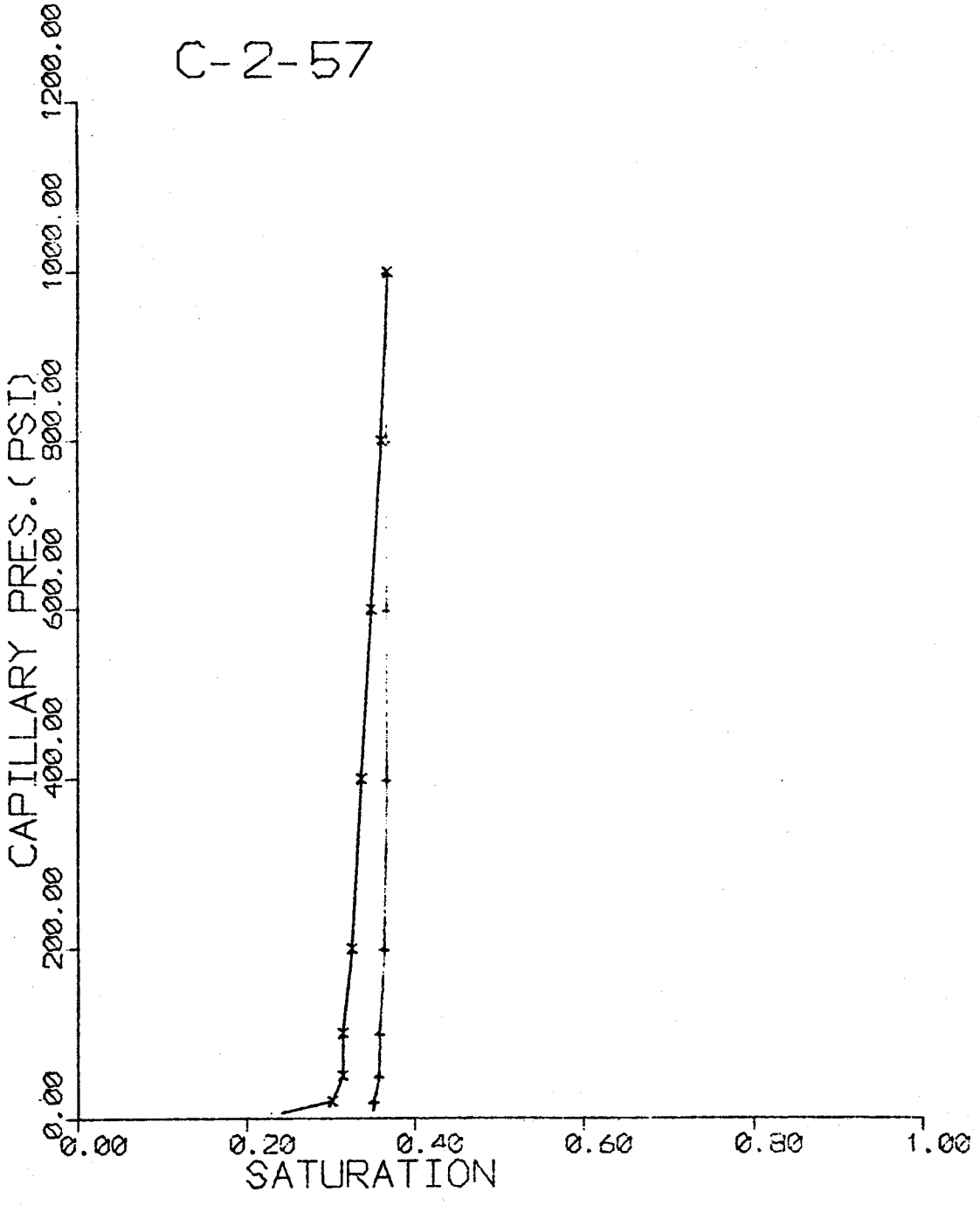

Figure 19

Experimental Capillary Pressure Curve for Sample C-2-57

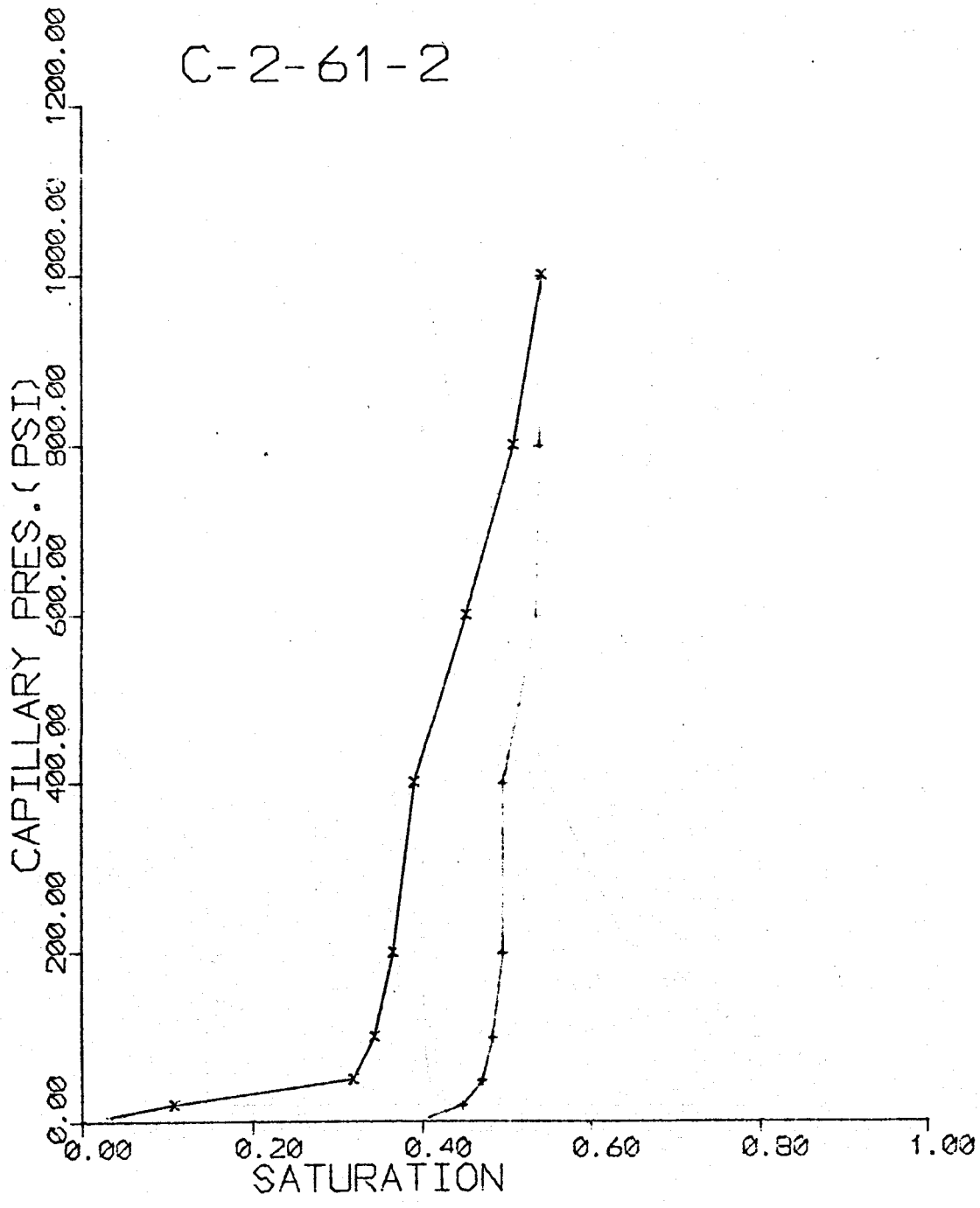

Figure 20

Experimental Capillary Pressure Curve for Sample C-2-61-2

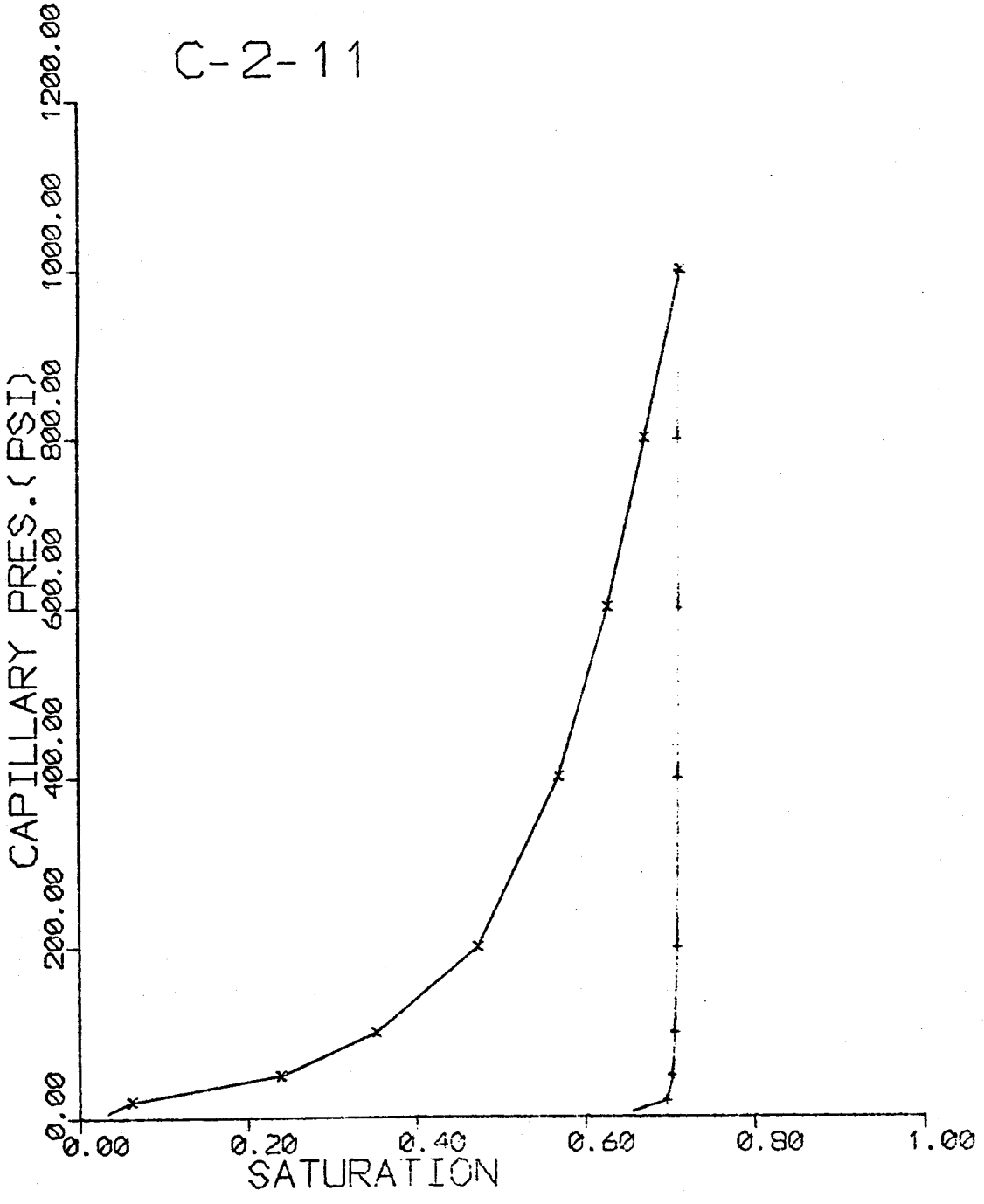

Figure 21

Experimental Capillary Pressure Curve for Sample C-2-11

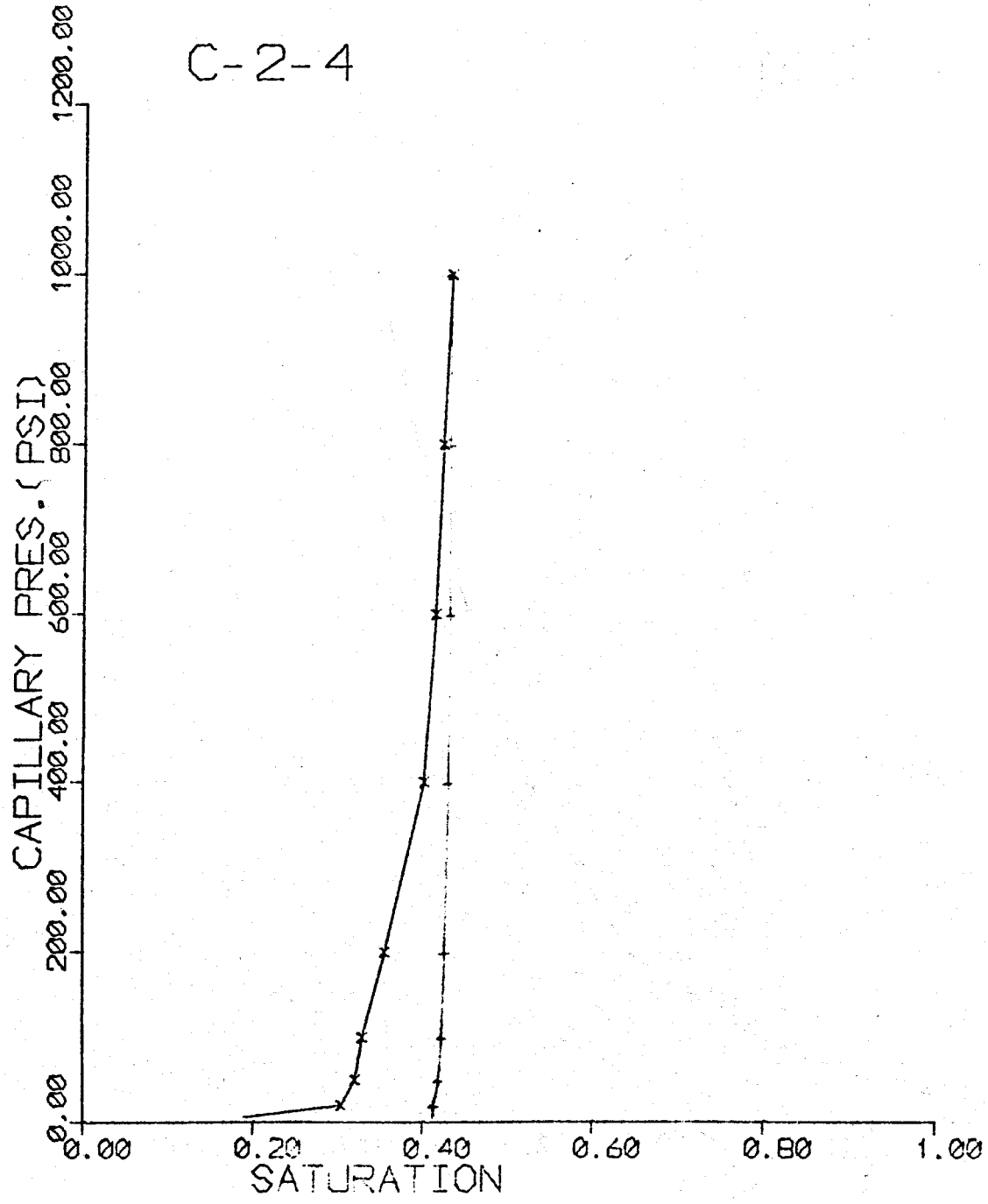

Figure 22

Experimental Capillary Pressure Curve for Sample C-2-4

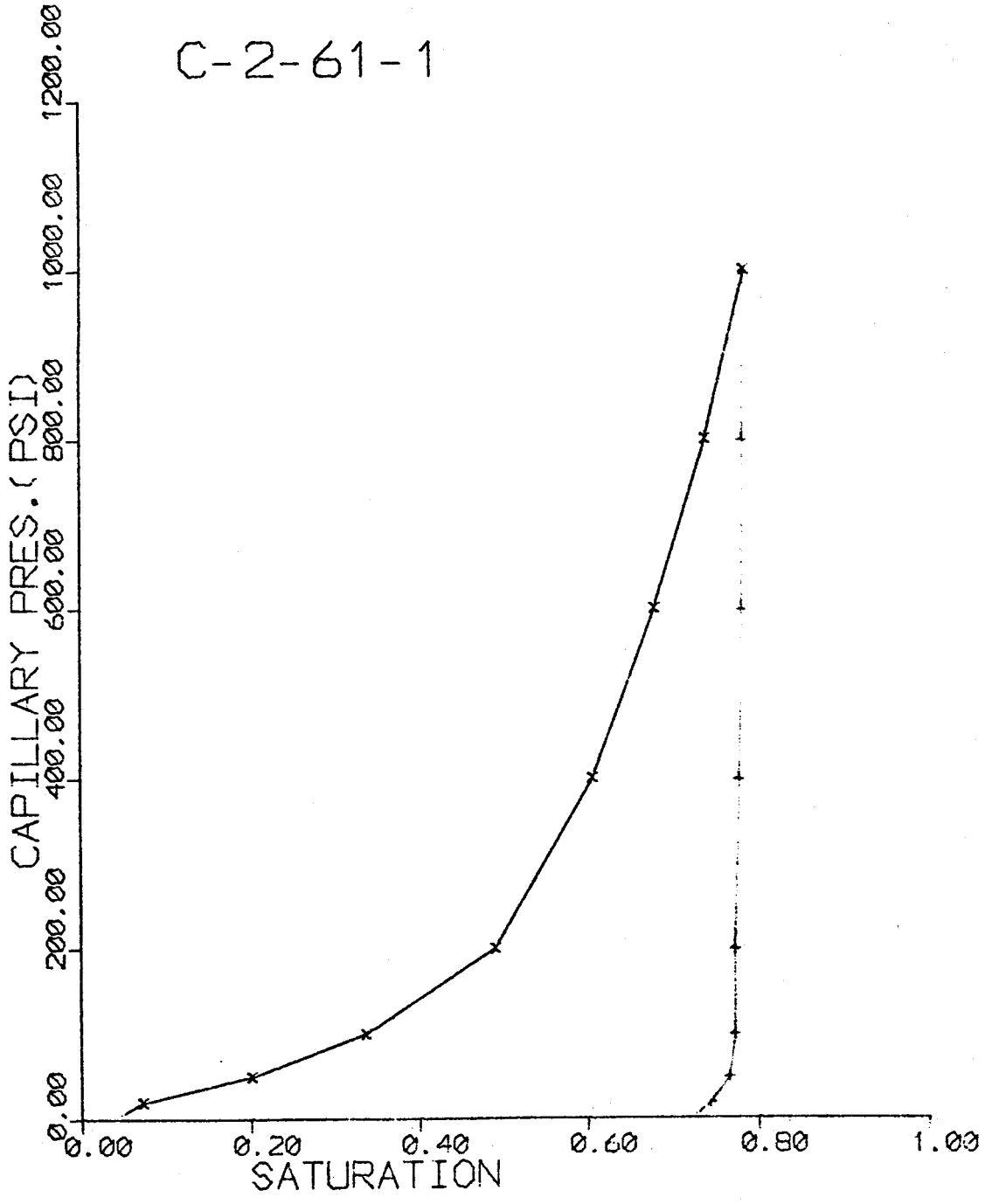

Figure 23

Experimental Capillary Pressure Curve for Sample C-2-61-1

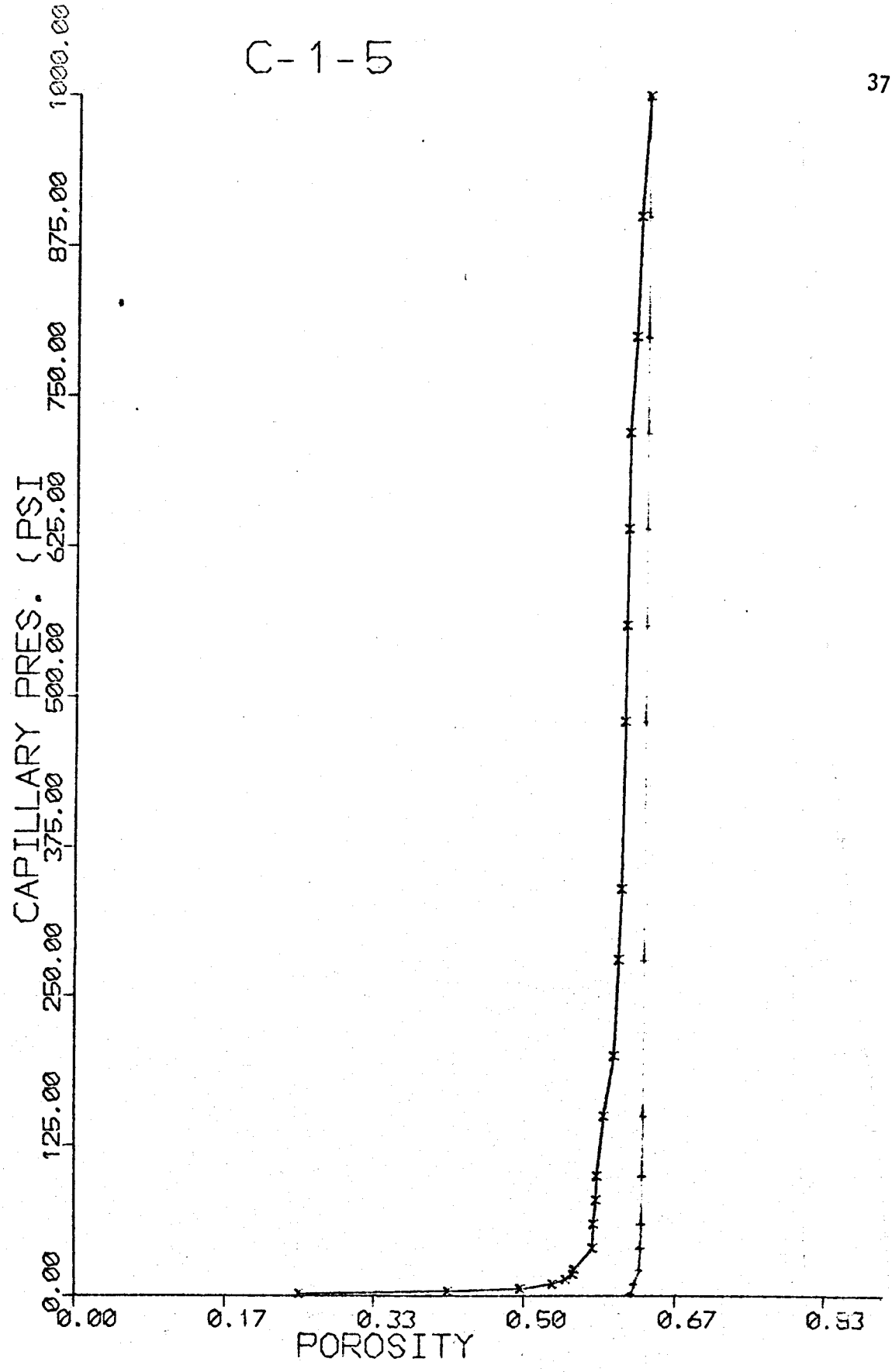

Figure 24

Experimental Capillary Pressure Curve for Sample C-1-5

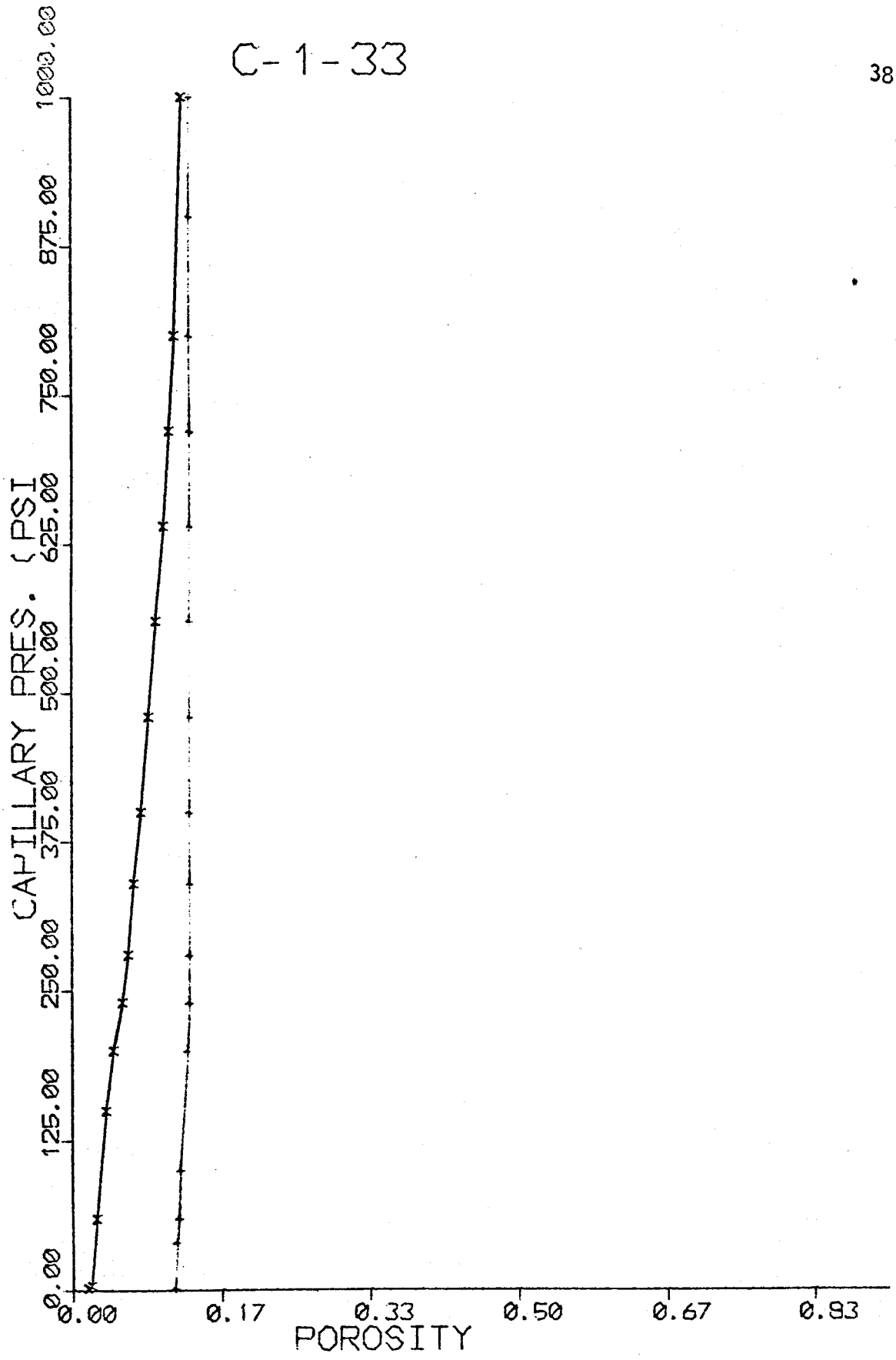

Figure 25

Experimental Capillary Pressure Curve for Sample C-1-33

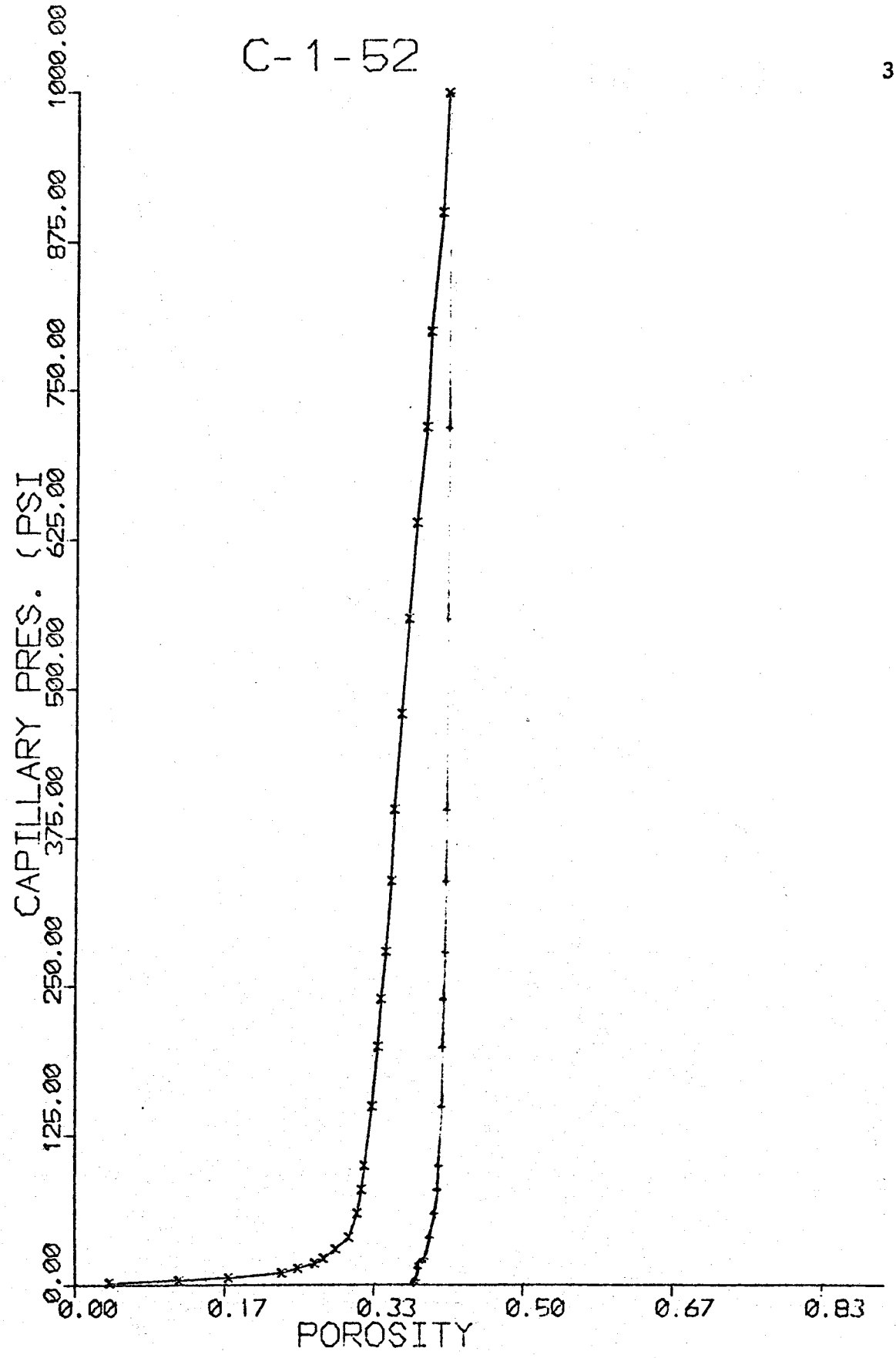

Figure 26

Experimental Capillary Pressure Curve for Sample C-1-52

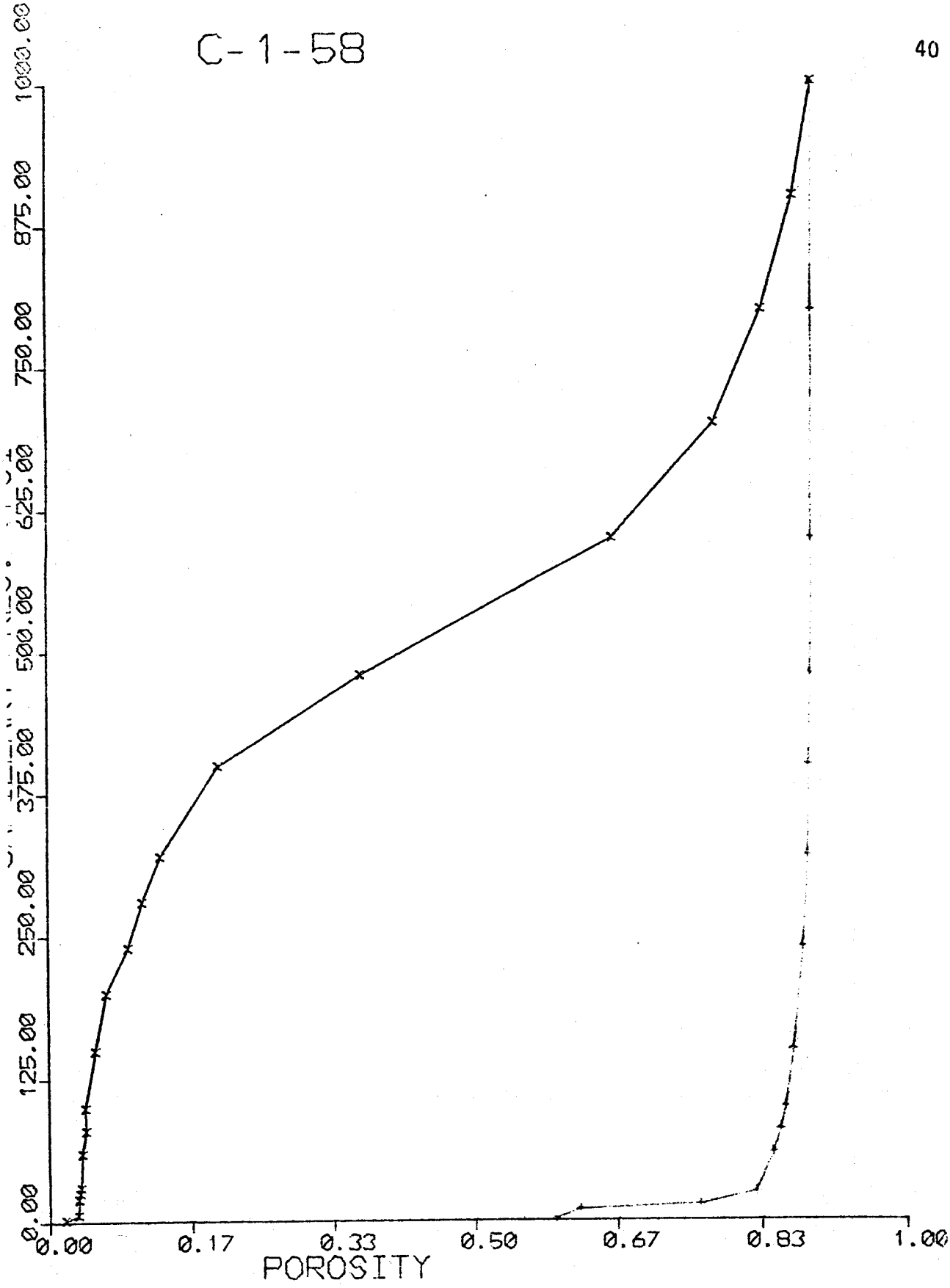

Figure 27

Experimental Capillary Pressure Curve for Sample C-1-58

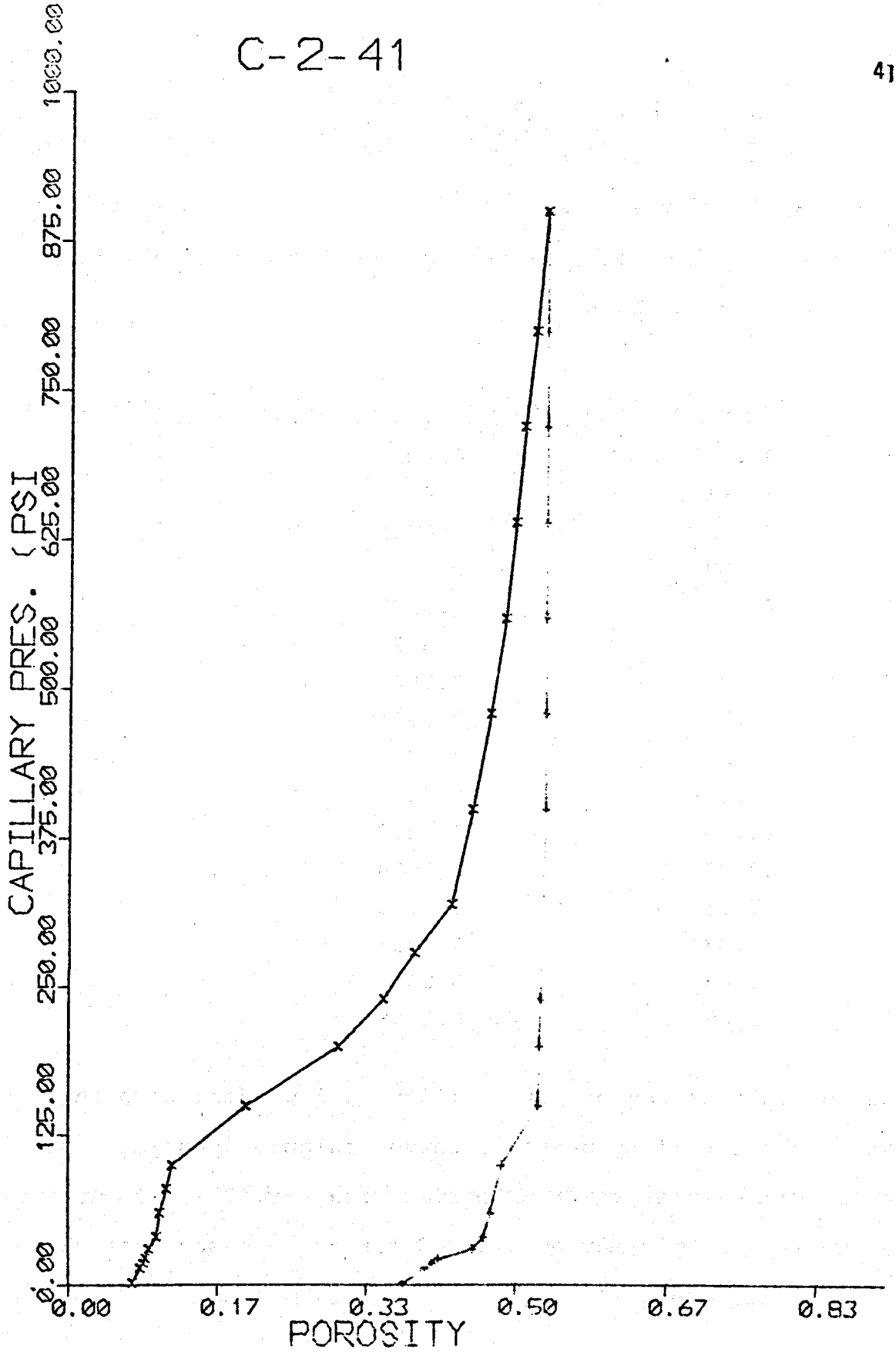

Figure 28

Experimental Capillary Pressure Curve for Sample C-2-41

S is mercury saturation

and P_c is capillary pressure.

The chart in Figure 45 lists the calculated permeabilities for 16 of the rock samples.

Sample	Porosity (%)	Theoretical Permeability (millidarcy)
C-2-11	37.34	0.8830
C-2-4	16.41	0.8980
C-2-57	21.05	0.6429
C-2-611	28.99	0.5540
C-2-612	28.56	1.3361
C-2-7	24.39	2.6077
C-1-33	7.0	0.1840
C-1-5	12.8	11.9571
C-1-58	9.2	0.5899
C-2-41	15.03	0.5313
NM-20	15.09	0.0209
NM-28	20.88	0.1990
NM-41	17.71	0.2626
OC-10	20.33	0.5055
OC-37	21.69	0.0130
OR-M	33.89	0.1498

Because the calculation of permeability is dependent upon the area under the capillary pressure curve, calculations were not attempted for the near vertical curves with very low saturation, such as C-1-45, but it may be assumed for these cases that the permeability is very small.

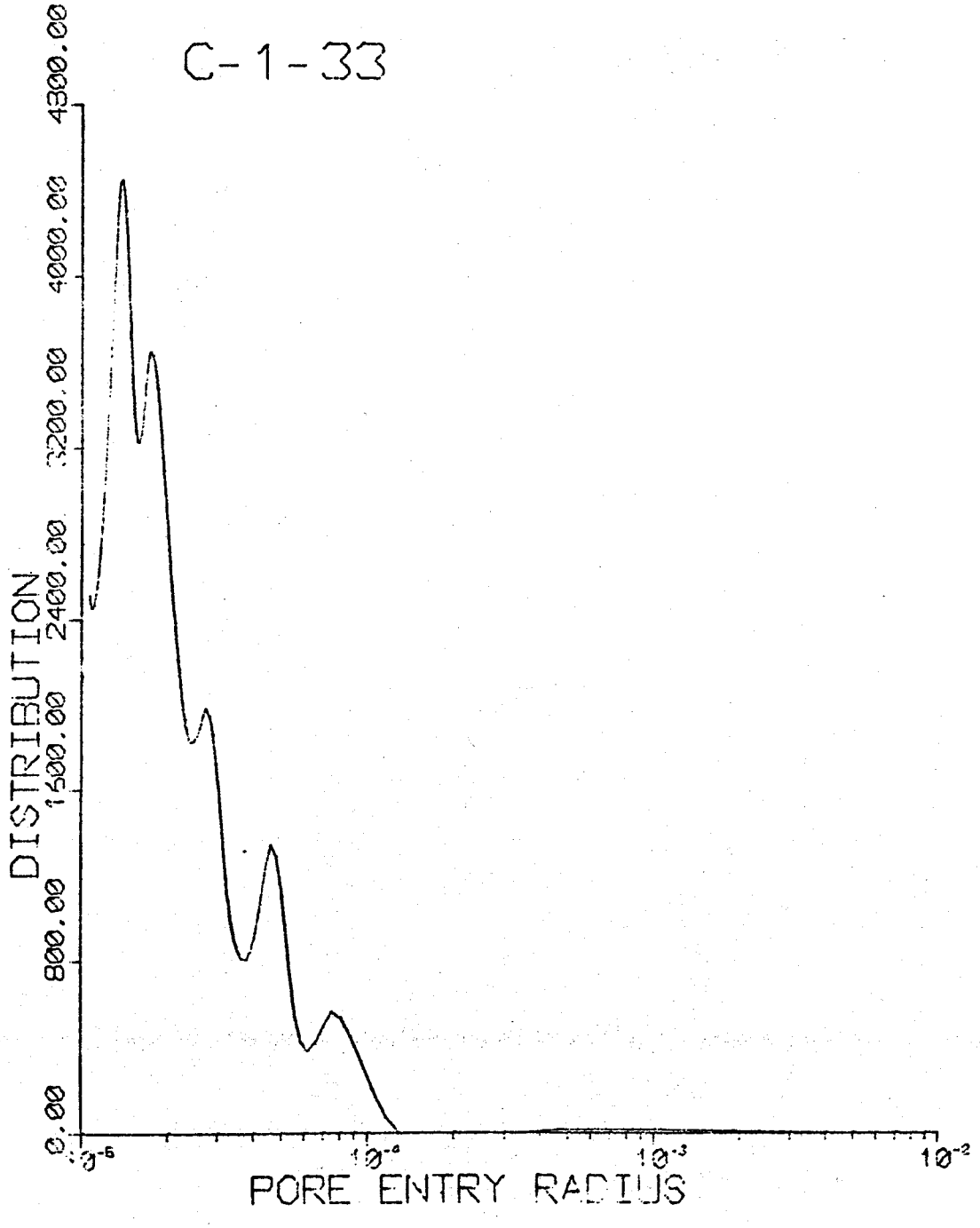

Figure 29

Pore Size Distribution Curve for Sample C-1-33

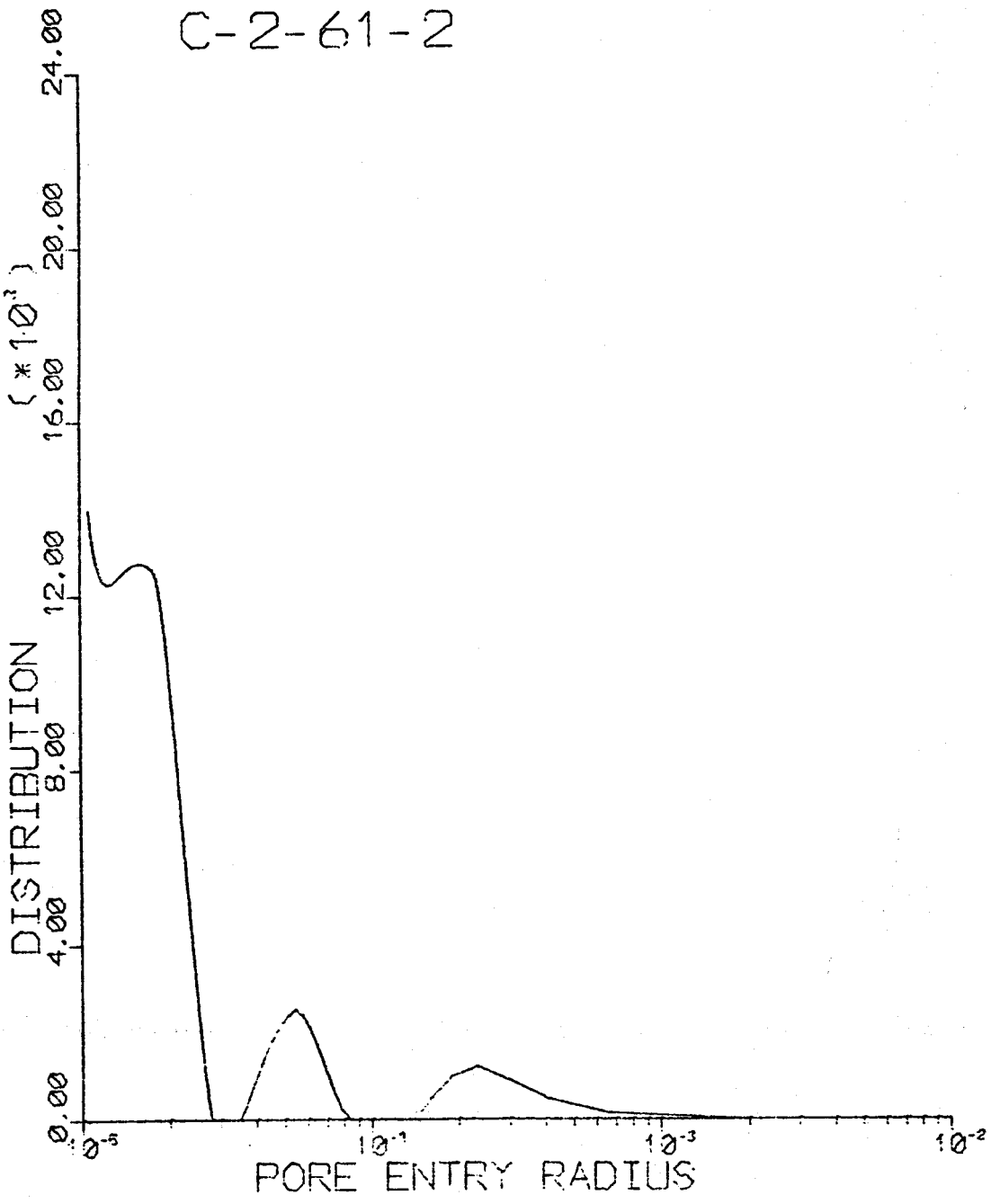

Figure 30

Pore Size Distribution Curve for Sample C-2-61-2

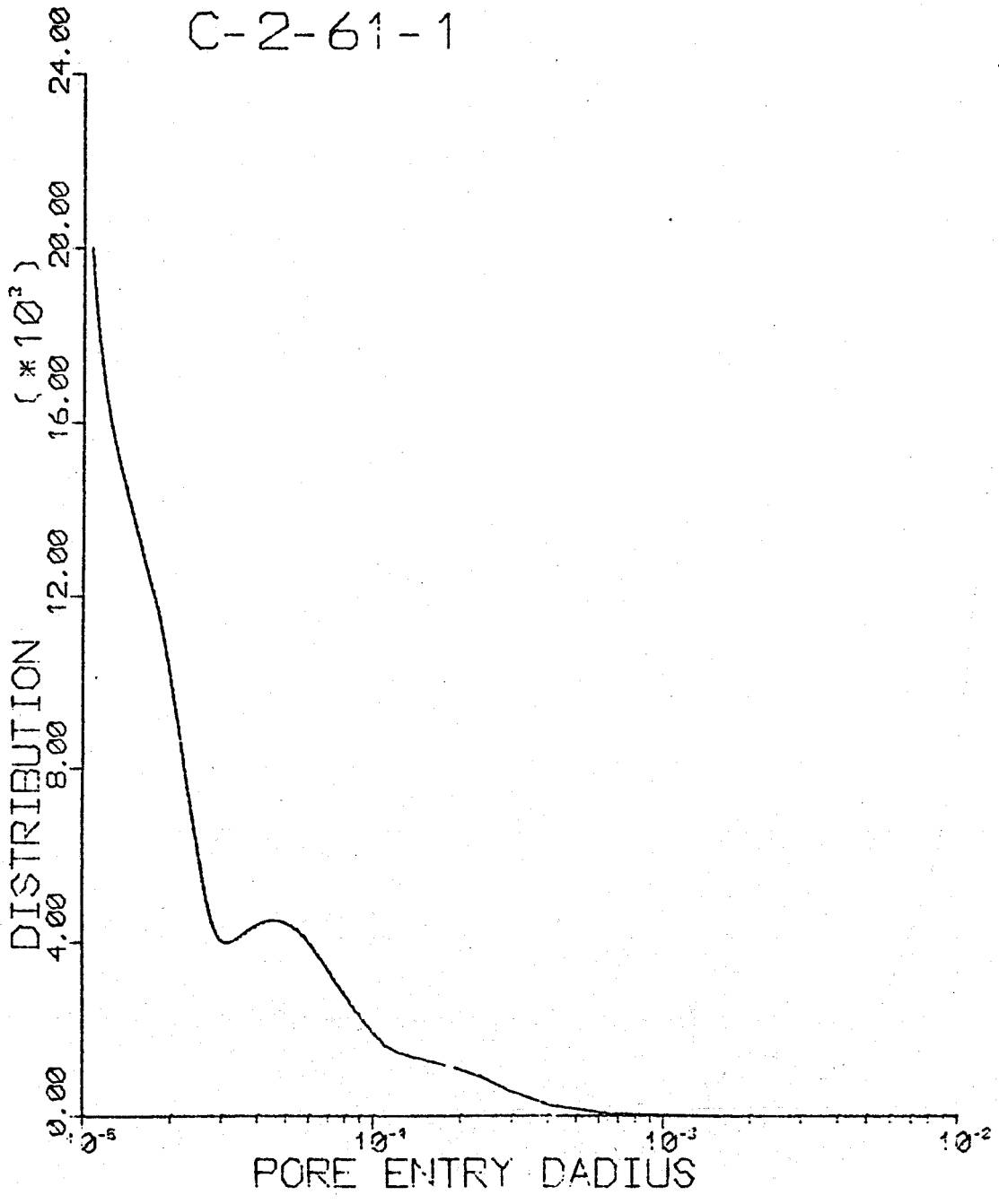

Figure 31

Pore Size Distribution Curve for Sample C-2-61-1

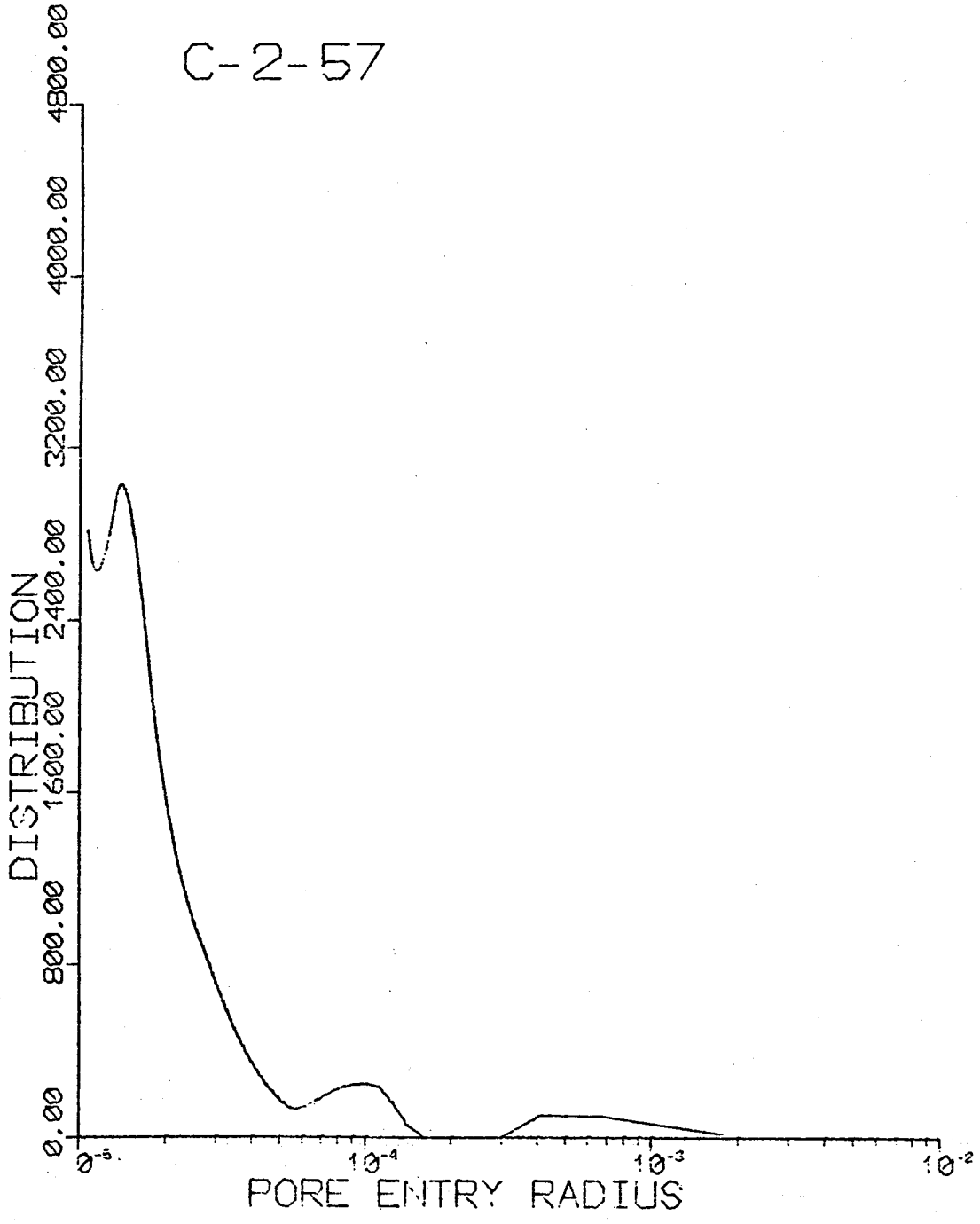

Figure 32

Pore Size Distribution Curve for Sample C-2-57

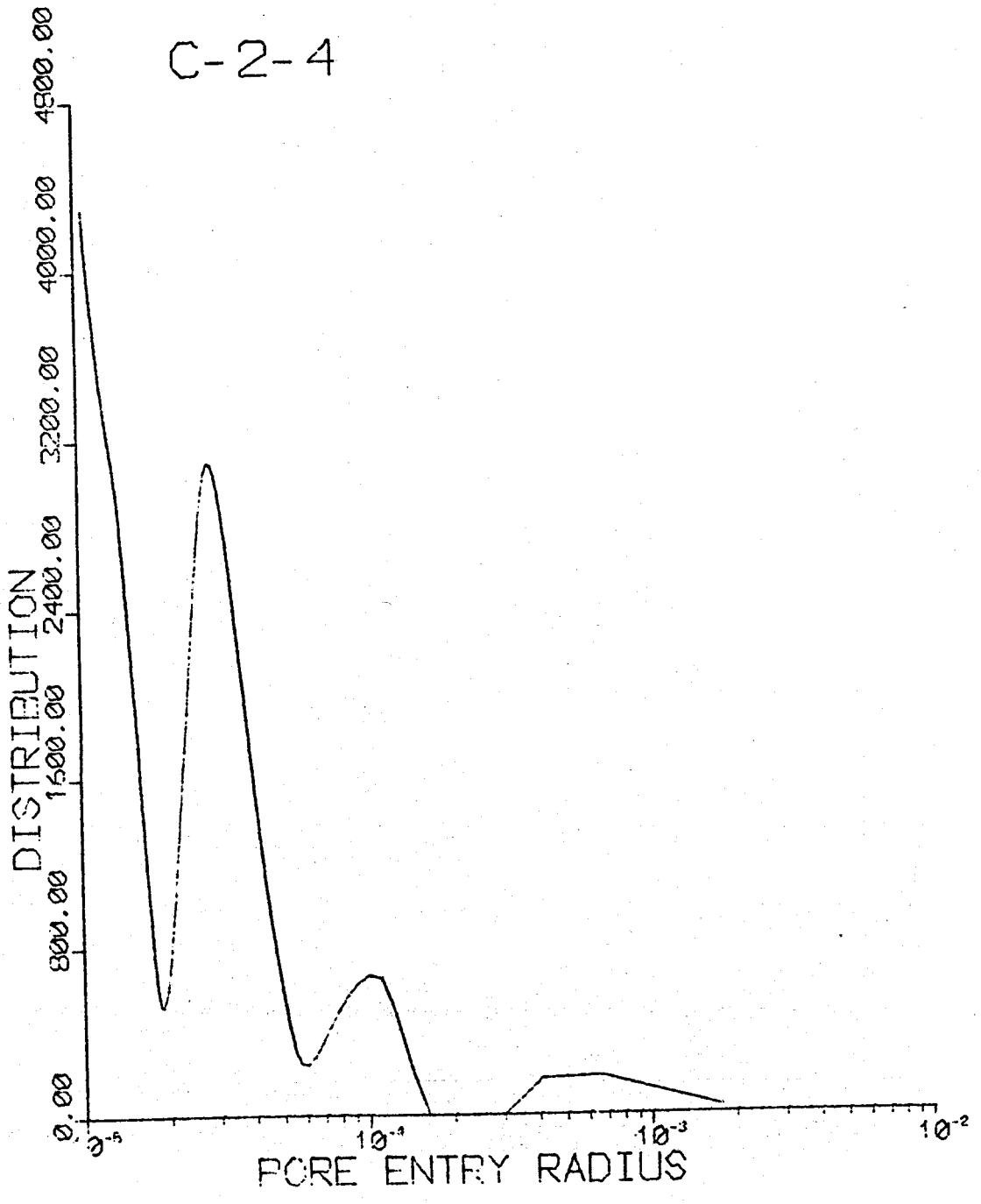

Figure 33

Pore Size Distribution Curve for Sample C-2-4

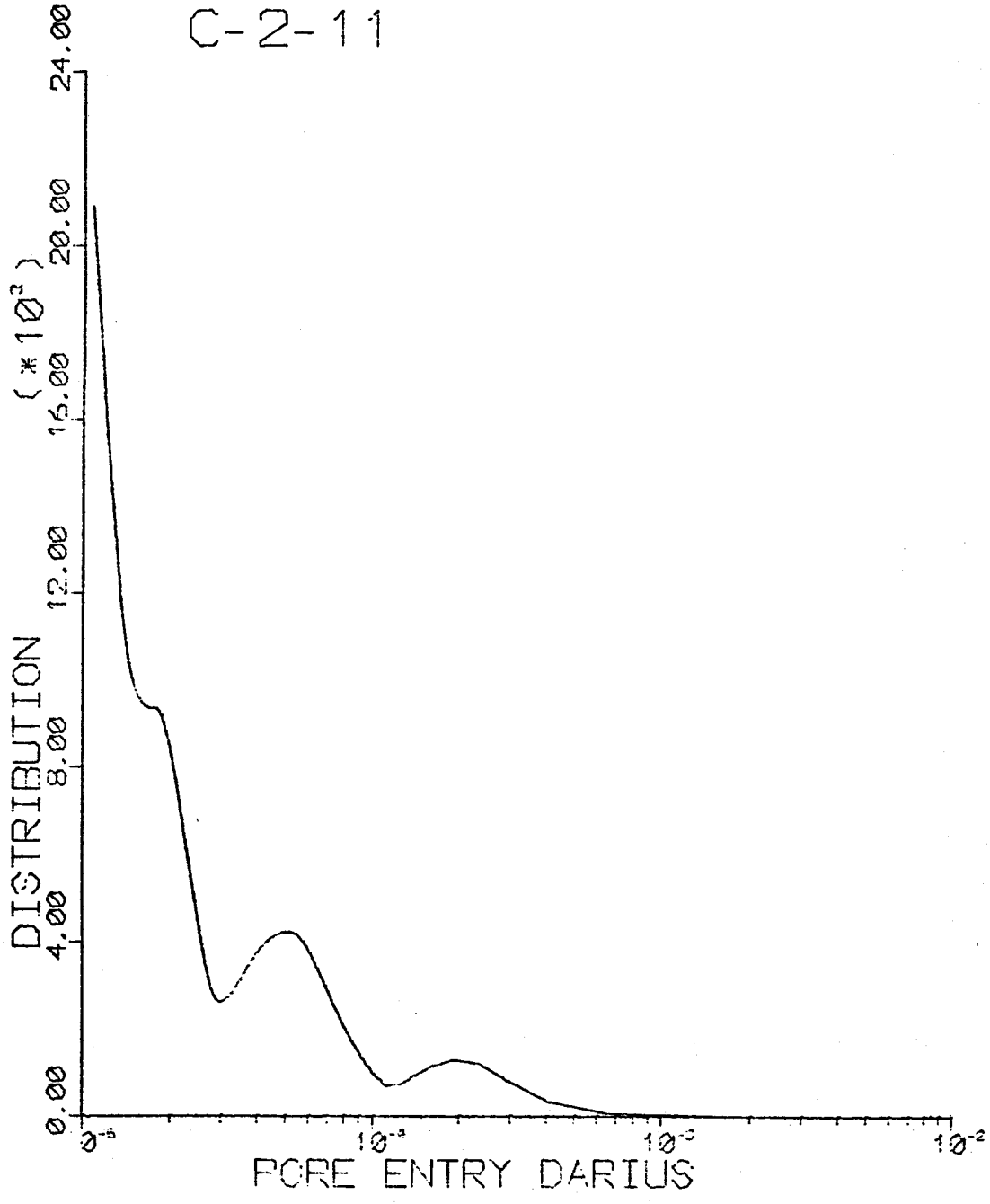

Figure 34

Pore Size Distribution Curve for Sample C-2-11

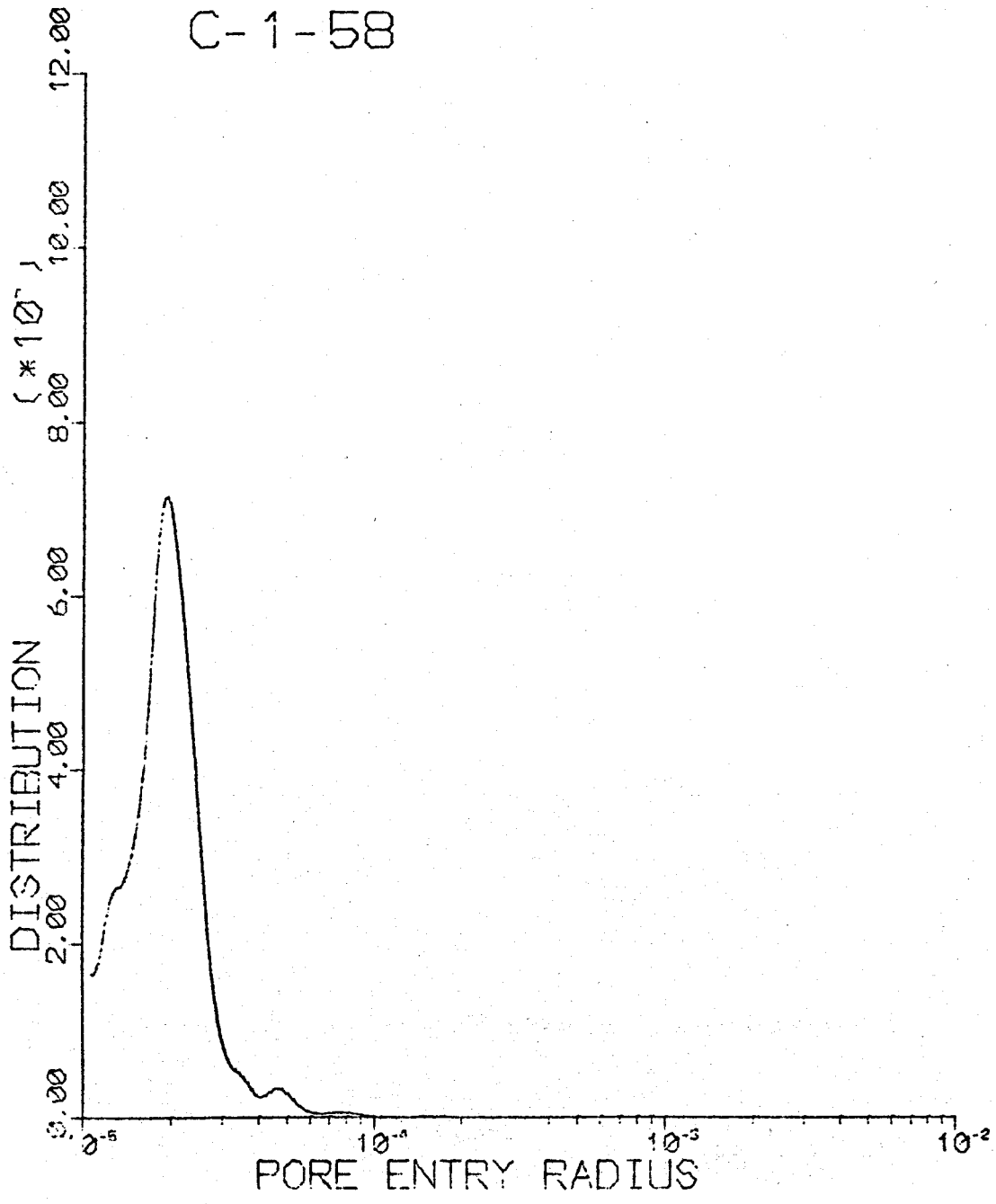

Figure 35

Pore Size Distribution Curve for Sample C-1-58

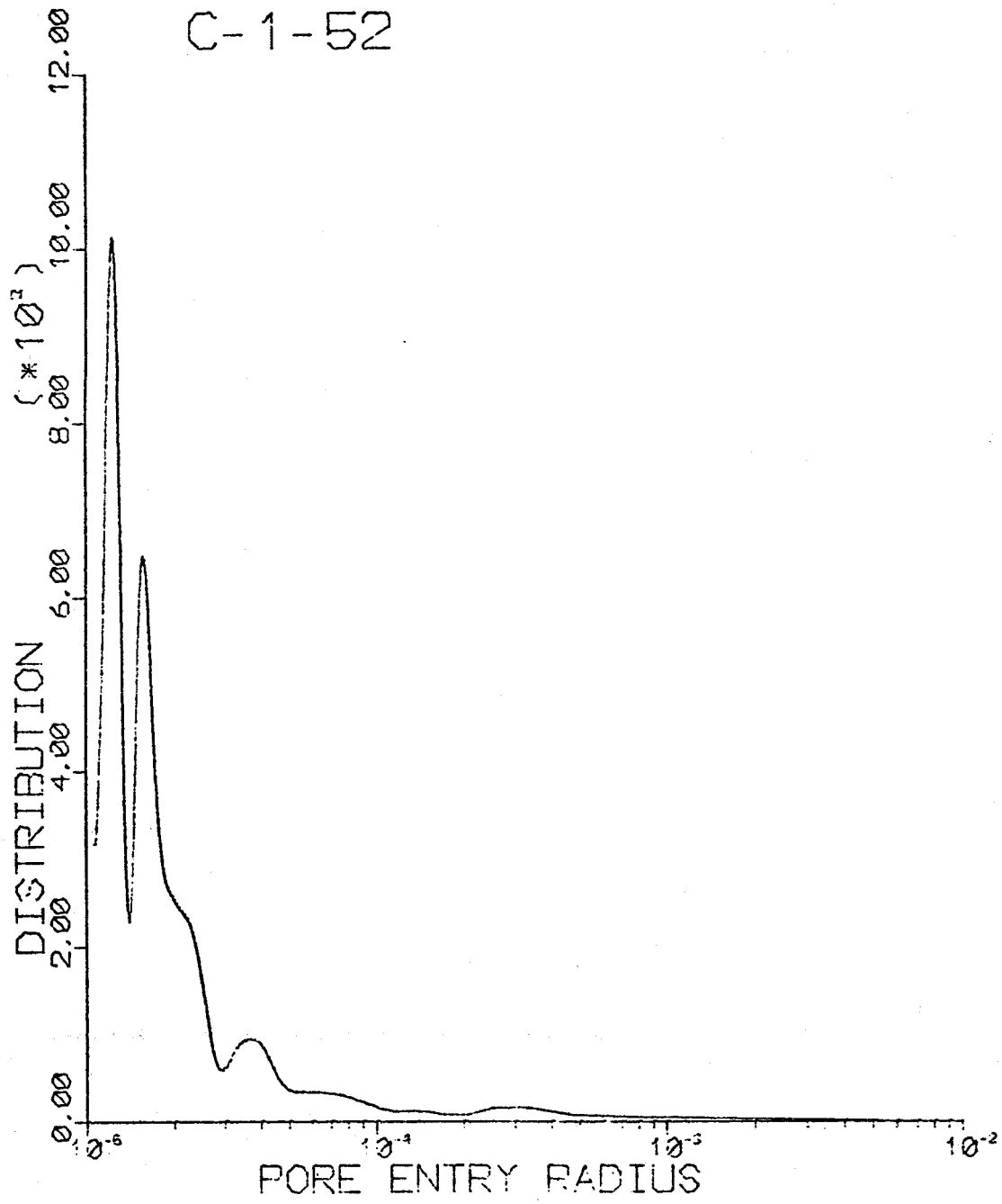

Figure 36

Pore Size Distribution Curve for Sample C-1-52

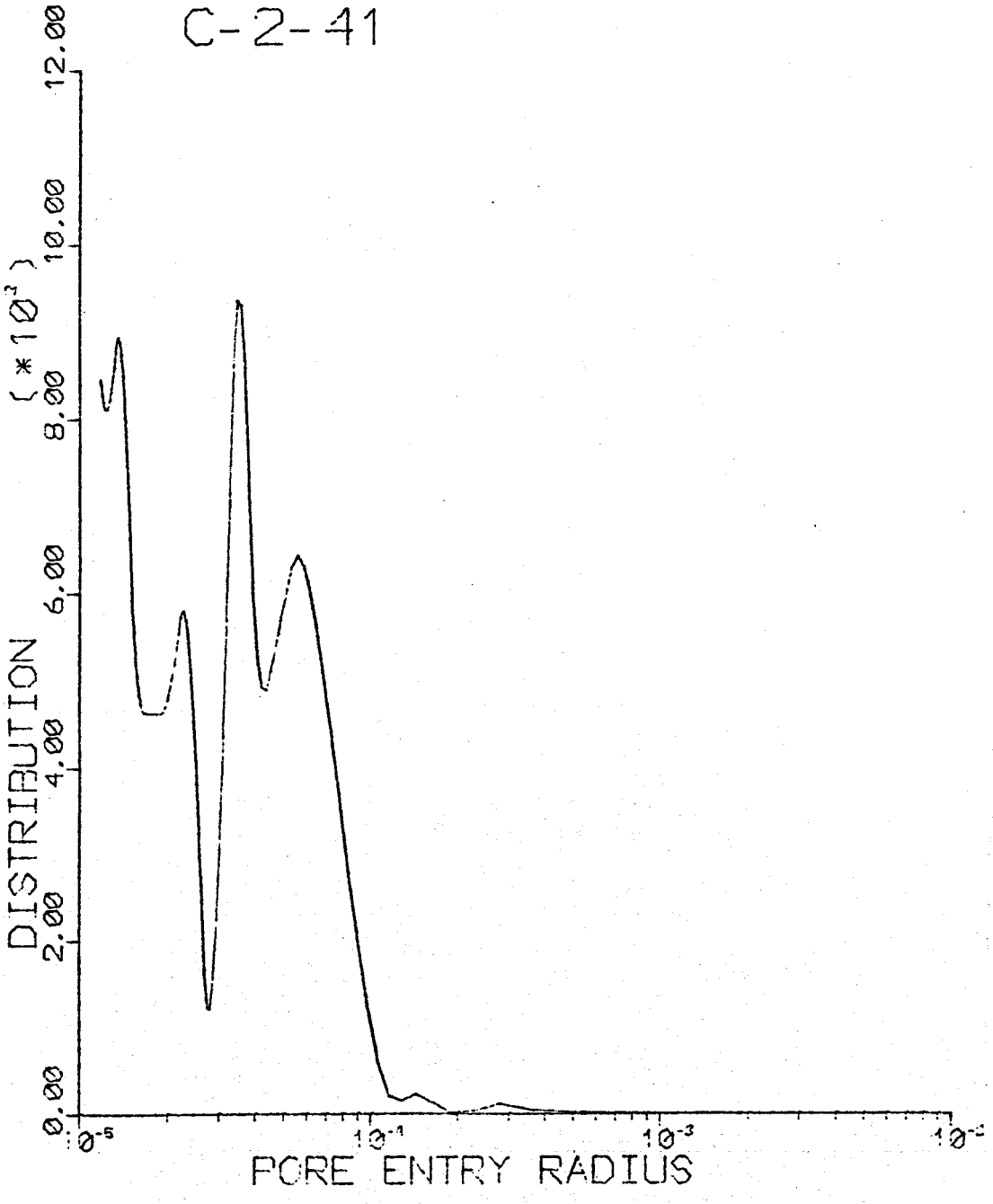

Figure 37

Pore Size Distribution Curve for Sample C-2-41

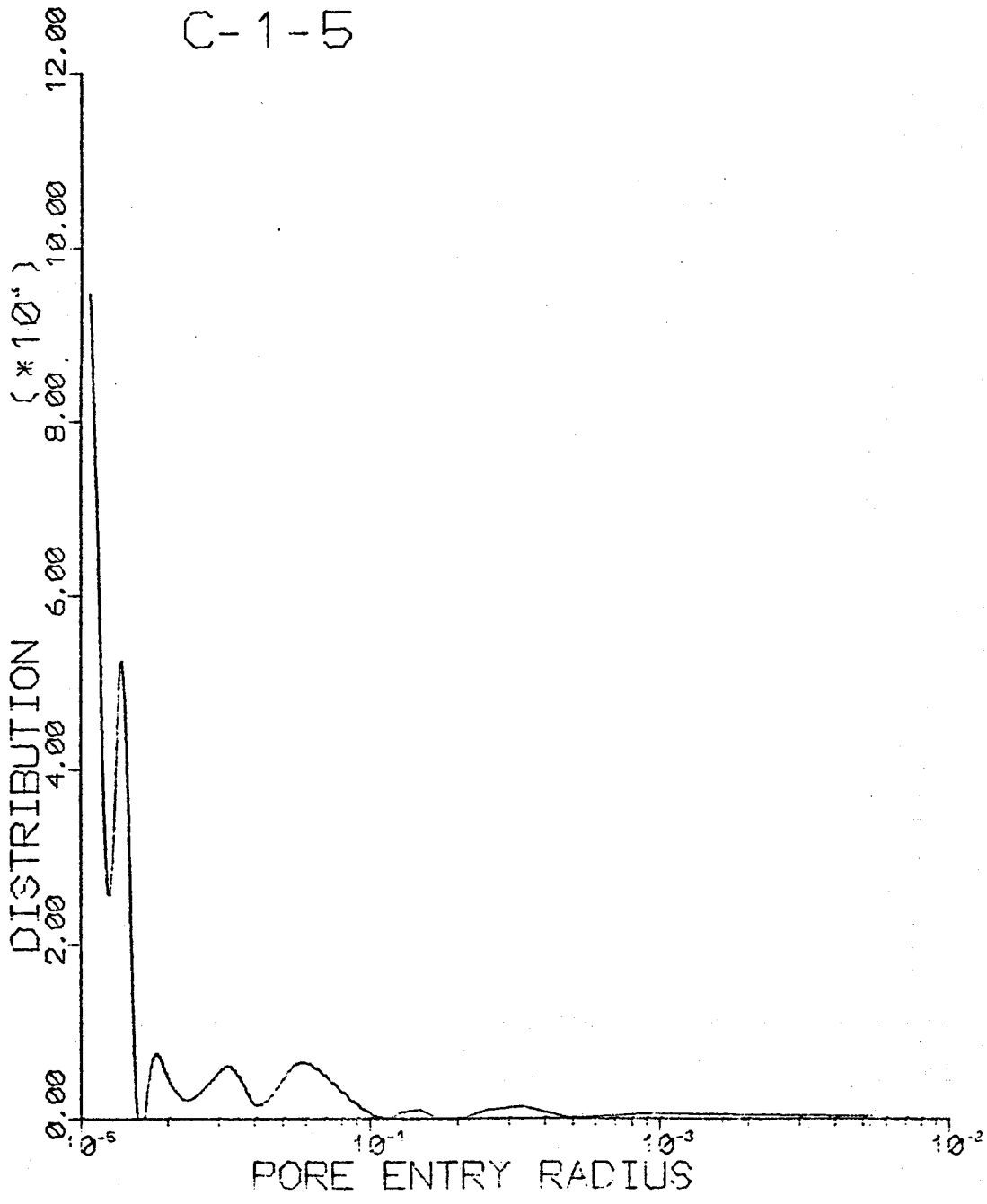

Figure 38

Pore Size Distribution Curve for Sample C-1-5

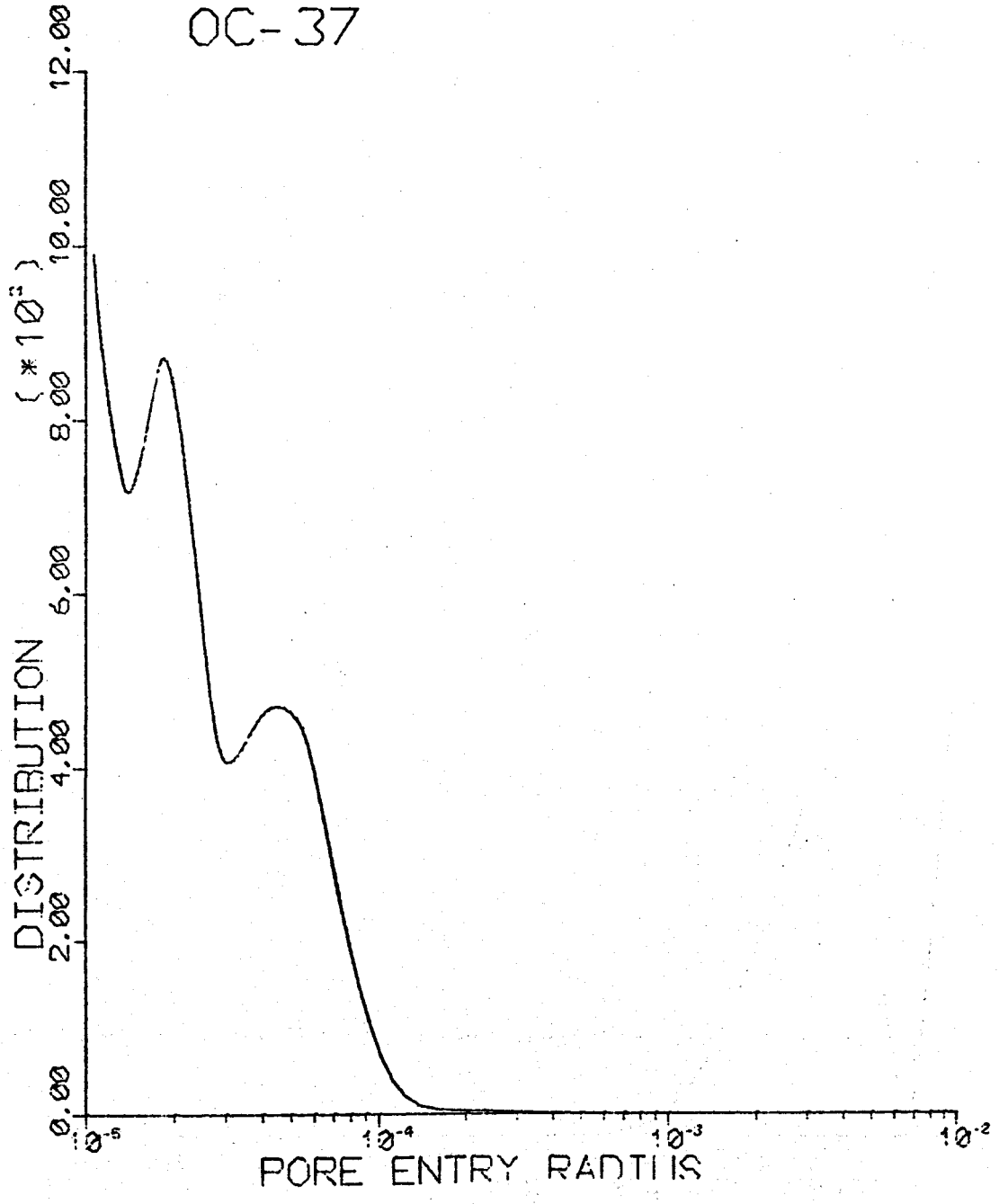

Figure 39

Pore Size Distribution Curve for Sample OC-37

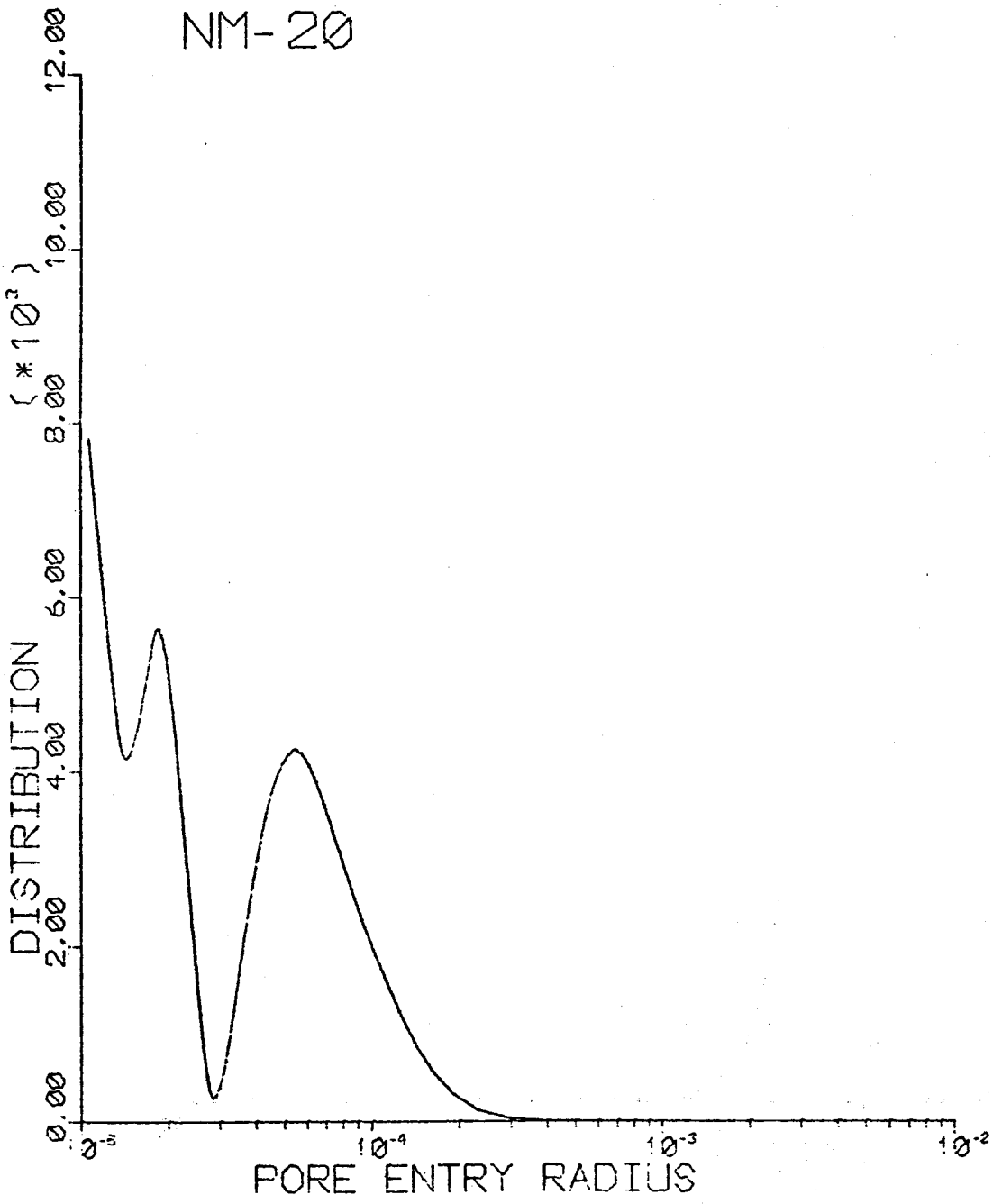

Figure 40

Pore Size Distribution Curve for Sample NM-20

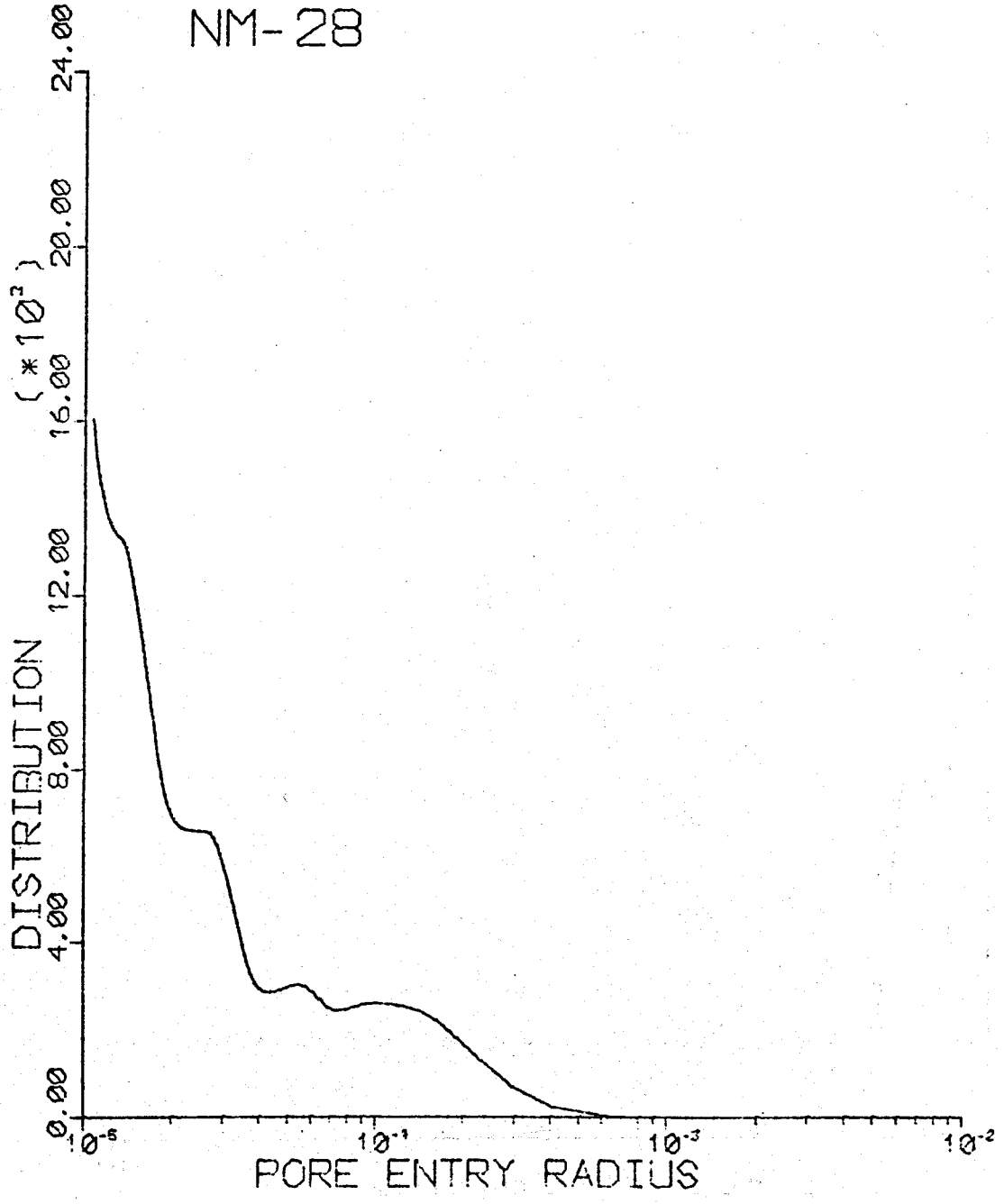

Figure 41

Pore Size Distribution Curve for Sample NM-28

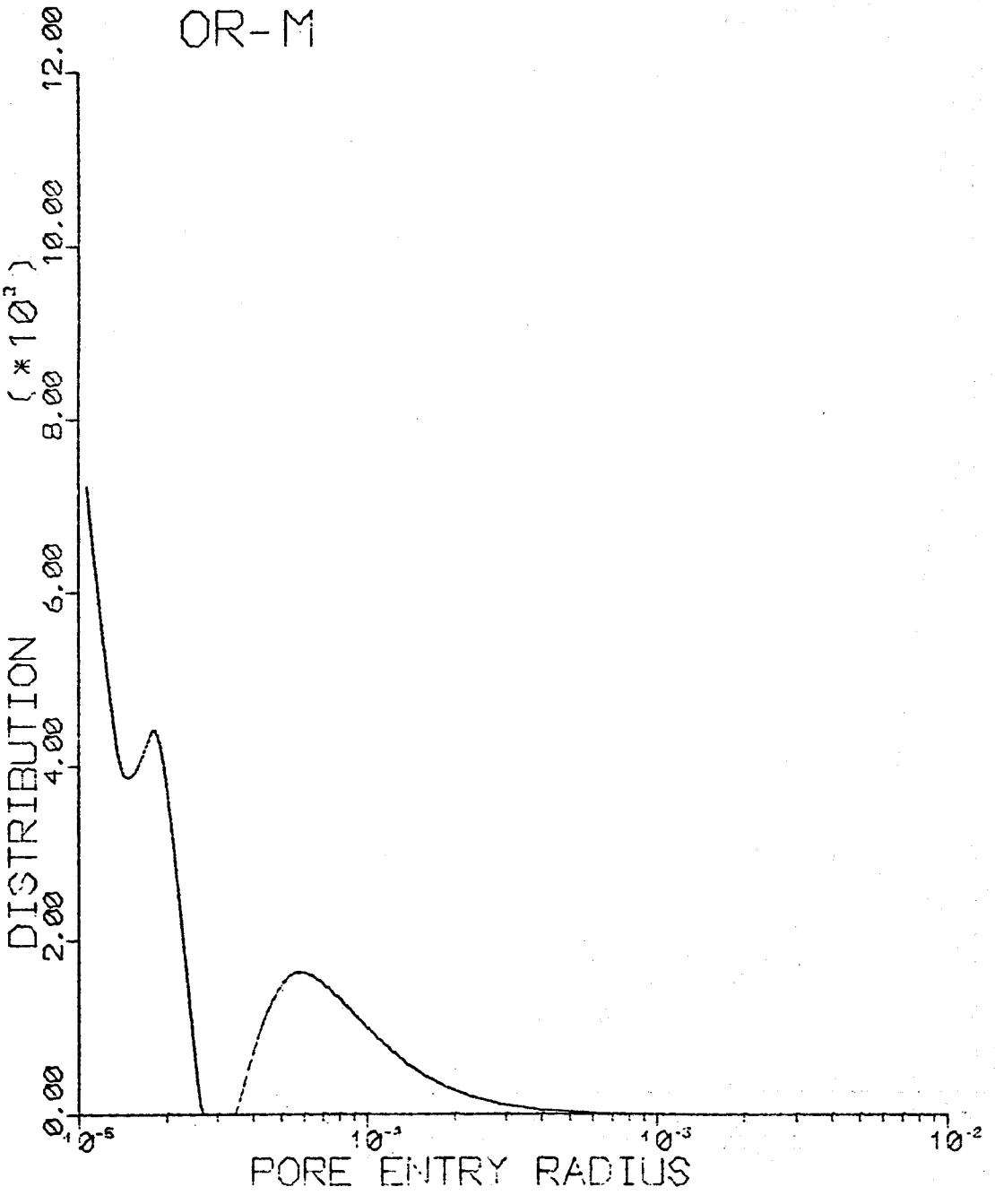

Figure 42

Pore Size Distribution Curve for Sample OR-M

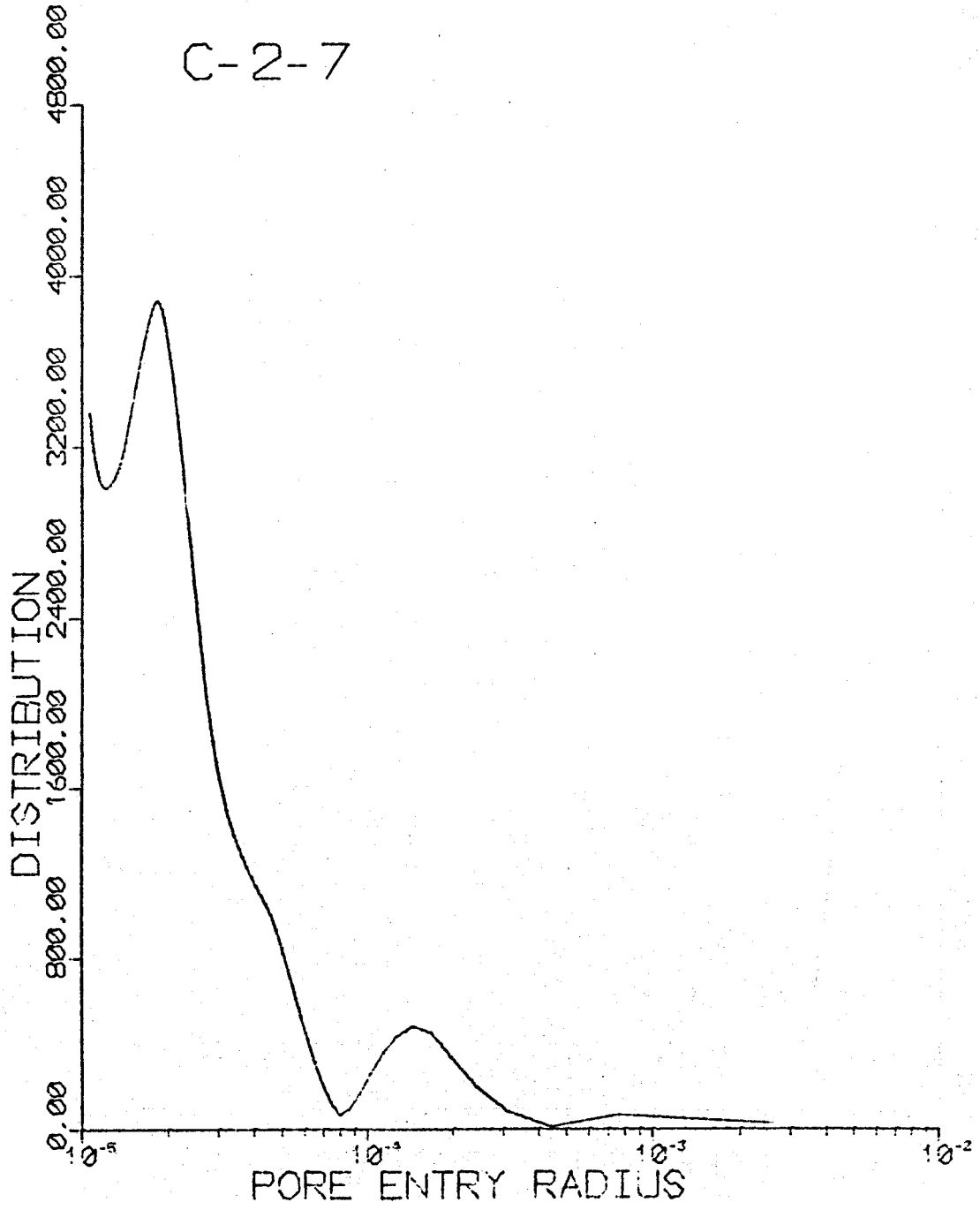

Figure 43

Pore Size Distribution Curve for Sample C-2-7

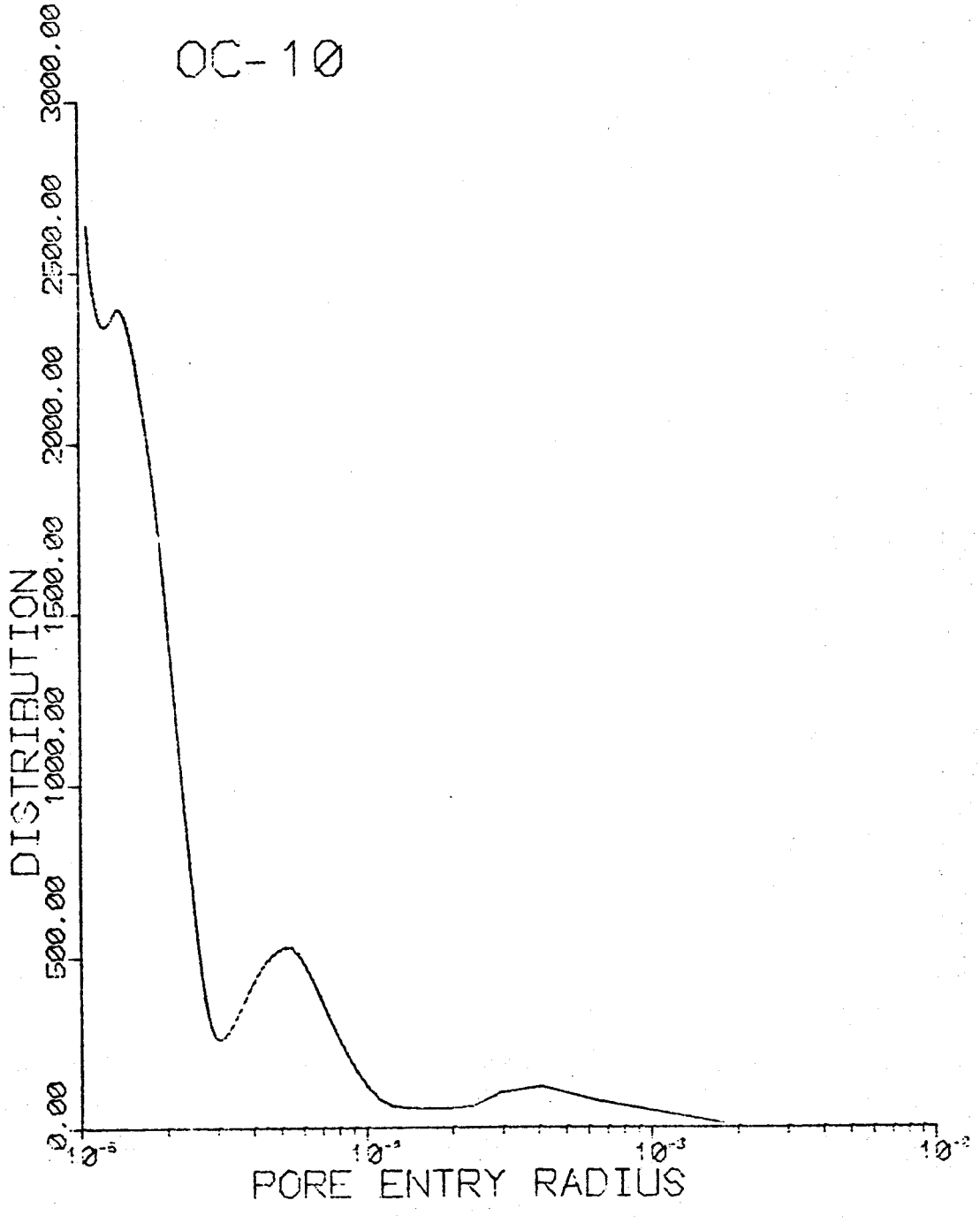

Figure 44

Pore Size Distribution Curve for Sample OC-1Ø

CONCLUSIONS AND FUTURE RECOMMENDATIONS

THERMAL CONDUCTIVITY MEASUREMENTS

After construction and testing of a flash technique to measure thermal conductivity of rock samples it was found to be fast and accurate. The successful system is now ready to measure additional samples. In the future, it is hoped to replace the flash tube with a lasar source which would concentrate more energy on the sample. Measurements with the lasar are also to be extended to higher temperatures and pressures to better study the range of conditions found in a geothermal reservoir.

CAPILLARY PRESSURE MEASUREMENTS

Variations in pore structure was noted by measurement of capillary pressure curves but more samples must be run to note a pattern between pore structure and such rock properties as seismic velocities and resistivities.

Considerable scatter in the velocity versus porosity curve for rock suite C (Columbia Plateau Volcanic Basin) was noted. Therefore capillary pressure measurements have been concentrated on this particular group. It is hoped that with additional samples, a pattern between pore structure and velocity will emerge.

Kwon (1975) has developed a relationship between formation factor and capillary pressure curves by statistical means. With additional capillary pressure curves, a better understanding of resistivity measurements should therefore result.

Finally, it has been found that the mercury injection technique works well only for rocks of higher porosity. For rocks with porosities of less

than 10%, a brine-air technique must be used. Equipment to complete these measurements is "on-order" and upon its arrival, the measurements will begin on tight samples. Purcell (1949) has discussed the relationship between mercury/air and brine/air techniques and therefore a comparison in the two types of curves can be made.

REFERENCES

Adams, M., 1954, Thermal Conductivity: III, Problate Spheroidal Envelope Method, Journal of the American Ceramic Society, v. 37, no. 2, p. 74-79.

Beck, A.E., 1976, An improved method of computing the thermal conductivity of fluid-filled sedimentary rocks, Geophysics, v. 41, p. 133-144.

Birch, F., and H. Clark, 1940, The thermal conductivity of rocks and its dependence upon temperature and composition, part I, Am. Jour. Sci., v. 238, p. 529-553.

Blackwell, J.H., 1956, The Axial-Flow Error in the Thermal-Conductivity Probe, Canadian Journal of Physics, v. 34, p. 412-417.

Clark, H., 1941, The effect of simple compression and wetting on the thermal conductivity of rocks, Trans. Am. Geoph. Union, II, p. 543-544.

De Vries, D.A., 1952, Mededelingen van de landliouwhogenchord te wageningen.

Hutt, J.R., and J.W. Berger, Jr., 1968, Thermal and electrical conductivities of sandstone rocks and ocean sediments, Geophysics, v. 33, p. 489-500.

Ibrahim, Electrical and Thermal Properties of Geothermal Reservoir Rocks, Colorado School of Mines Proposal.

Jenkins, R.J., 1961, and W.J. Parker, 1961, A flash method for determining thermal diffusivity over a wide temperature range, Wadd Technical Report 61-95, U.S. Naval Radiological Defense Laboratory.

Kuni, D., and J.M. Smith, 1960, Heat transfer characteristics of porous rocks, J. Am. Inst. Ch. Eng., v. 6, p. 71-77.

Kwon, Bong Sung, 1975, A mathematical pore structure model and pore structure interrelationships, CSM Thesis 1717.

Maxwell, J.C., 1904, A treatise on electricity and magnetism, 3rd ed., Clarendon Press, Oxford.

Parker, W.J., R.J. Jenkins, C.P. Butler, and G.L. Abbott, 1961, Flash method of determining thermal diffusivity, heat capacity, and thermal conductivity, J. App. Phy., v. 32, p. 1679-1684.

Pickett, G.R., Class Notes for Well Logging [GP 532] Course, C.S.M.

Purcell, W.R., 1949, Capillary pressures -- their measurement using mercury and the calculation of permeability therefrom: Petroleum Trans., AIME, T.P. 2544, p. 39-48.

Ruska Mercury -- Injection Capillary Pressure Apparatus Model 1057 Users Manual.

Russell, H.W., 1935, Principles of heat-flow in porous insulation, J. Am. Cer. Soc., v. 18, p. 1-5.

Sass, J.H., A.H. Lachenbruck, R.J. Munroe, 1971, Thermal Conductivity of Rocks from Measurements on Fragments and its Application to Heat-Flow Determinations, Journal of Geophysical Research, v. 76, no. 14, p. 3391-3401.

Sugarwara, A., and Y. Yoshizawa, 1962, An experimental investigation on the thermal conductivity of consolidated porous materials, J. Appl. Phy., v. 33, p. 3135-3138.

Walsh, J.B., and E.R. Decker, 1966, Effect of pressure and saturating fluid on the thermal conductivity of compact rock, J. Geoph. Res., v. 71, p. 3053-3061.

Woodside, W., and J.H. Messmer, 1961, Thermal conductivity of porous media I. unconsolidated sands, J. Appl. Phy., v. 32, p. 1688-1698.

_____ , and _____ , 1961, Thermal conductivity of porous media, II. consolidated rocks, J. Appl. Phy., v. 32, p. 1699-1706.

Wyllie, M.R.J., and P.F. Southwick, 1954, An experimental investigation of the self potential and resistivity phenomena in dirty sands, J. Pet. Tech., v. 6, p. 44-57.

Zierfriss, H., and G. Van der Vliet, 1956, Laboratory measurements of heat conductivity of sedimentary rocks, Bull. Am. Assoc. Pet. Geol., v. 40, p. 2475-2488.

☆U.S. GOVERNMENT PRINTING OFFICE: 1979-640-092/530